Global Biogeochemical Cycles

RESEARCH ARTICLE
10.1029/2020GB006603

Key Points:

- In a Global Ocean Biogeochemical Model, we simulate short continental shelf water residence times driven by dominant open ocean inflows
- These hydrodynamical features lead to net autotrophy and a slight sink of atmospheric CO_2 over the preindustrial global shelf
- The results also suggest that the global continental shelf is a less efficient sink of anthropogenic CO_2 than the open ocean

Supporting Information:

- Supporting Information S1

Correspondence to:
F. Lacroix,
fabrice.lacroix@mpimet.mpg.de

Citation:
Lacroix, F., Ilyina, T., Laruelle, G. G., & Regnier, P. (2021). Reconstructing the preindustrial coastal carbon cycle through a global ocean circulation model: was the global continental shelf already both autotrophic and a CO_2 sink?. *Global Biogeochemical Cycles*, *35*, e2020GB006603. https://doi.org/10.1029/2020GB006603

Received 19 MAR 2020
Accepted 18 JAN 2021

Reconstructing the Preindustrial Coastal Carbon Cycle Through a Global Ocean Circulation Model: Was the Global Continental Shelf Already Both Autotrophic and a CO_2 Sink?

Fabrice Lacroix[1,2,3], Tatiana Ilyina[1], Goulven G. Laruelle[2], and Pierre Regnier[2]

[1]Ocean in the Earth System, Max Planck Institute for Meteorology, Hamburg, Germany, [2]Department Geoscience, Environment & Society (DGES), Université Libre de Bruxelles, Brussels, Belgium, [3]Max Planck Institute for Biogeochemistry, Jena, Germany

Abstract The contribution of continental shelves to the marine carbon cycle is still poorly understood. Their preindustrial state is, for one, essentially unknown, which strongly limits the quantitative assessment of their anthropogenic perturbation. To date, approaches developed to investigate and quantify carbon fluxes on continental shelves have strongly simplified their physical and biogeochemical features. In this study, we enhance the global ocean biogeochemistry model HAMburg Ocean Carbon Cycle by explicitly representing riverine loads of carbon and nutrients, as well as improving the representation of organic matter dynamics in the coastal ocean. Our simulations, at a resolution of ~0.4°, reveal a globally averaged shelf water residence time (RT) of 12–17 months, which is much shorter than the global RTs previously assumed in benchmark studies (>4 years). This shorter global RT, induced primarily through outer shelf regions with large oceanic inflows, promotes an efficient offshore transport of terrestrial and marine organic carbon (0.44 $PgCyr^{-1}$) and a dissolved inorganic carbon sink from the organic cycling of carbon on the global shelf (net ecosystem productivity [NEP] equal to +0.20 $PgCyr^{-1}$). In turn, this autotrophic state of continental shelves contributes to a weak global preindustrial sink of atmospheric CO_2 (0.04 $PgCyr^{-1}$), dominated by extensive regions with large oceanic inflows and positive NEPs, such as the Patagonian shelf, the East China Sea and the outer North Sea. The contemporary global shelf CO_2 uptake of 0.15 $PgCyr^{-1}$ furthermoresuggests that the anthropogenic CO_2 uptake (0.11 $PgCyr^{-1}$) on the global continental shelf is less efficient with respect to the open ocean.

1. Introduction

In spite of their relatively small global surface coverage (~8% of the global ocean, Laruelle et al., 2013), continental shelves are believed to contribute disproportionally to the global oceanic primary production, as well as to the global carbon burial (Andersson et al., 2005; Chen & Borges, 2009; Gattuso et al., 1998; Mackenzie et al., 2004, 1998, 2000; Milliman & Droxler, 1996; Muller-Karger et al., 2005; Walsh, 1991; Wollast & Chou, 1998). The quantification of carbon cycling on the shelves, however, remains entailed with large uncertainties. Most prominently, the net ecosystem productivity (NEP) and air-sea CO_2 exchange (FCO_2) over continental shelves have been a matter of intense debate (Andersson et al., 2005; Bauer et al., 2013; Borges et al., 2005; Bourgeois et al., 2016; Cai, 2011; Chen & Borges, 2009; Crossland et al., 2006; Laruelle et al., 2018, 2014; Mackenzie et al., 2004, 1998, 2000; Regnier et al., 2013; Roobaert et al., 2019).

The NEP of continental shelves is defined as the difference between gross primary production (GPP) and net ecosystem respiration (NER). In simple terms, the GPP is limited by light, temperature and the availability of nutrients (R. C. Smith et al., 1987; Tyrrell, 1999), while the NER is largely controlled by the amount, composition, and chemical reactivity of terrigenous and autochthonous organic matter, as well as by the availability of oxidants (Arndt et al., 2013; Cai et al., 1999; S. V. Smith & Hollibaugh, 1993).

For contemporary conditions, Bauer et al. (2013) have suggested that continental shelves are weakly autotrophic (NEP > 0), globally, while regional observational studies have shown that the trophic state of coastal waters may significantly differ in sign and magnitude from one region to another (Anderson et al., 2009; Borges et al., 2005; Thomas et al., 2005). Conceptual box model studies, such as those of Mackenzie

et al. (2004, 1998, 2000), Rabouille et al. (2001), and Andersson et al. (2005), have suggested that, under preindustrial conditions, global continental shelves were net heterotroph (NEP < 0) due to their processing of terrestrially derived organic matter, but that the marked historical coastal fertilization through increases in riverine nutrient supplies pushed the trophic state of the global shelf toward net autotrophy over the past century. It was, however, also acknowledged by Andersson et al. (2005) that the representation of the global continental shelf in these models as a single, perfectly mixed water body characterized by residence times (RTs) of 4–10 years was a strong simplification, which certainly impacted the simulated carbon dynamics on the shelf. For instance, the RTs of continental shelf waters, which are important control factors of the intensity of coastal biogeochemical processing (Borges et al., 2005; Cai, 2011; Fennel & Testa, 2019), including the degradation of terrestrial organic matter (Painter et al., 2018) and the export rates of nutrients from the coastal ocean to the open ocean (Izett & Fennel, 2018; Sharples et al., 2017), are spatially strongly variable (Izett & Fennel, 2018; Liu et al., 2019; Sharples et al., 2017).

In stark contrast to the continental shelf NEP, which cannot be quantified from observations alone, the present-day air-sea CO_2 flux (FCO_2) over continental shelves has been improvingly constrained in quantitative terms as a result of the compilation of large observational databases of oceanic pCO_2 data, such as SOCAT (Bakker et al., 2016). On the basis of these databases, the contemporary continental shelf CO_2 sink has been estimated in the range of 0.14–0.25 $PgCyr^{-1}$ (Laruelle et al., 2014; Roobaert et al., 2019). However, the estimation of the preindustrial FCO_2, which is needed to quantify the anthropogenic perturbation of the continental shelf FCO_2, can presently only be assessed through model realizations. In conceptual box model studies (Andersson et al., 2005; Mackenzie et al., 2004, 2000), continental shelves were found to be a global preindustrial source of atmospheric CO_2 in the range of 0.1–0.3 $PgCyr^{-1}$, but they were suggested to progressively switch to a contemporary sink of 0.1–0.4 $PgCyr^{-1}$ over the 20th century, suggesting an anthropogenic CO_2 sink of up to about 0.7 $PgCyr^{-1}$. This would represent a much higher anthropogenic carbon uptake per area with respect to the open ocean. This strong FCO_2 trend thereby partly mirrored the simulated switch in sign of the continental shelf NEP, thus these studies identified the biological carbon pump on the global shelf as a dominant driver of the anthropogenic FCO_2. These findings are partly supported by the observation-based study of Laruelle et al. (2018), which reports an increasing efficiency of the continental shelf CO_2 sink over the last three decades in several large coastal regions and, thus, a strong anthropogenic perturbation of the shelf FCO_2 over this recent multidecadal period, an efficient sink explained by short shelf water turnover times in the study. The perturbation of the 20th century continental shelf FCO_2 was also recently investigated in a three dimensional (3D)-resolving Global Ocean Biogeochemical Model (GOBM) study by Bourgeois et al. (2016), a study that revealed that the anthropogenic perturbation of the global shelf CO_2 uptake might only be of 0.1 $PgCyr^{-1}$. Critically, however, an initial preindustrial state was not achieved in these GOBM simulations, which were forced by increasing atmospheric CO_2 concentrations. Starting from a likely strongly drifting initial state derived from present-day observations could potentially affect the responses of the nonlinear biogeochemical system to changes in atmospheric CO_2 concentrations.

Among the different approaches used to quantitatively constrain the continental shelf NEP and FCO_2, mass balance approaches (e.g., Gattuso et al., 1998) have provided useful insights regarding the magnitude of carbon fluxes and inventories at global and regional scales. Such simple approaches, however, do not provide a mechanistic description of relevant physical and biogeochemical processes, and fail to resolve the temporal evolution of the fluxes. Conceptual box models, by contrast, provide a comprehensive process-based description of carbon transport and transformations on the global continental shelf, but these models do not represent spatial features of the highly heterogeneous coastal ocean. Regional ocean circulation models have also been used to resolve heterogeneous coastal systems (Fennel & Wilkin, 2009; Frischknecht et al., 2018; Gruber et al., 2011), yet they do not provide a global perspective. GOBMs have, in the past, only provided a coarse representation of spatial features on continental shelves (Bernard et al., 2011; Lacroix et al., 2020) and/or relied on strongly simplified process representations of the biogeochemical cycling in these environments (Bourgeois et al., 2016), such as riverine inputs of carbon and nutrients.

In this manuscript, we make use of recent improvements to the HAMburg Ocean Carbon Cycle (HAMOCC) GOBM to perform simulations at a higher spatial resolution than is usually used in GOBM assessments of the oceanic carbon cycle, albeit the resolution is still coarse compared to the configurations of regional models (e.g., Frischknecht et al., 2018). In addition, we also use recent observation- and model-based

assessments of the spatio-temporal variability of key carbon fluxes and processes (e.g., coastal pCO_2, Laruelle et al., 2017; dynamics of terrestrial organic matter in the ocean, Aarnos et al., 2018) and in the sediment (Arndt et al., 2013) to improve the representation of biogeochemical processing taking place in the coastal ocean in HAMOCC. With this enhanced model, we aim to reconstruct the global shelf NEP and FCO_2 at preindustrial conditions. We address the following research questions:

- What is the mean simulated global shelf water RT and how do the spatial RT fields compare to previously reported values derived from observational data and regional models?
- What were the global preindustrial continental shelf NEP and FCO_2, and what controls their spatial distributions?
- What do these results imply for the anthropogenic FCO_2 perturbation when taking the present-day FCO_2 range into account?

2. Methods

2.1. Simulation Strategy

To simulate the physical and biogeochemical dynamics of continental shelf waters and sediment, we used a GOBM that was extended to incorporate an improved representation of biogeochemical cycling at the coastal system's interfaces (Figure 1a). The GOBM was, on one hand, coupled to a land-surface scheme that provided spatially resolved riverine inputs, including terrestrial dissolved organic matter (tDOM). On the other hand, fluxes at the pelagic-benthic interface of the model were altered to account for the efficient biogeochemical processing of organic matter taking place on continental shelves. Taken that the degradability of tDOM and of sedimentary organic matter in the coastal ocean are poorly constrained at the global scale, we performed a series of simulations to account for uncertainties in degradation rates found in literature and used the best rate estimate from those simulations for the main preindustrial simulation. We then performed a preindustrial baseline simulation of 1,500 years, in which the physical state of the ocean was driven by atmospheric data of ERA-20C data 20th century reanalysis (Poli et al., 2016), repeating over the years 1905–1930 of the data set. Furthermore, the atmosphere was prescribed a constant atmospheric CO_2 concentration (278 ppm, corresponding to the reference year 1800, Etheridge et al., 1996) and the last 100 years of the simulation were used to quantify preindustrial fluxes. This simulation time period was amply sufficient to achieve a biogeochemical state close to equilibrium on the global continental shelf, since the atmosphere, water column and sediment are closely linked in these systems. Starting from the preindustrial state, we performed a transient simulation from 1800 to 2015 with increasing atmospheric CO_2 concentrations (from 278 to 399 ppm, Etheridge et al., 1996), in order to assess the performance of the model versus present-day observational data, as well as to estimate the magnitude of the anthropogenic FCO_2 perturbation. We note that neither changes in oceanic circulation nor in riverine nutrient loads were considered in the transient simulation of this study.

2.2. Description of the Standard Ocean Model and Its Forcing

The physical fields which advect, mix and diffuse biogeochemical compounds were computed by the Max Planck Institute Ocean Model (MPI-OM), which is a z-coordinate ocean general circulation model that solves primitive equations under the hydrostatic and Boussinesq approximation on a C-grid and a free surface (Jungclaus et al., 2013). The grid configuration used in this study was the TP04 configuration of ~0.4° resolution for the main preindustrial and transient simulations, although different degradation rates of tDOM and sedimentary particulate organic matter (POM) were tested at a spatial resolution of 1.5° (GR15 configuration, Supporting Information S3). Vertically, the model comprises 40 uneven layers that increase in thickness with depth.

HAMOCC represents both the organic and inorganic cycling of carbon (Ilyina et al., 2013). The representation of organic cycling is based on a nutrients, phytoplankton, zooplankton, and detritus/POM type approach, with the addition of an in situ produced dissolved organic material pool (mDOM; Six & Maier-Reimer, 1996) and of N-fixating cyanobacteria (Paulsen et al., 2017). Phytoplankton takes up inorganic nutrients and carbon following the modified Redfield ratio of C:N:P = 122:16:1 (Takahashi et al., 1985) in the presence of sufficient light and nutrients (DIP, DIN, and DFe). Marine organic matter is exuded during

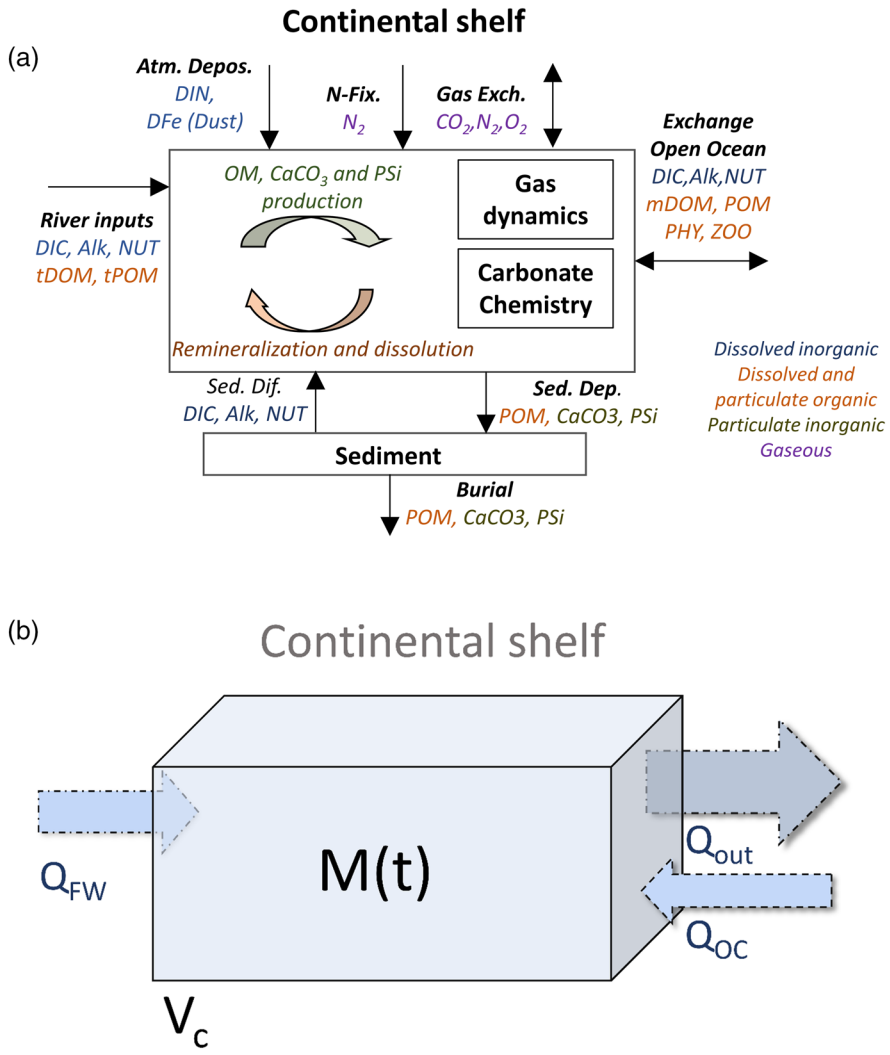

Figure 1. (a) Representation of continental shelves in the framework of this study's GOBM. At the land-sea interface, riverine inputs of key organic and inorganic compounds are constrained according to Lacroix et al. (2020). Within the water column, organic matter, calcium carbonate ($CaCO_3$), and opal (PSi) are produced biologically, and are recycled back to inorganic compounds via remineralization and dissolution. The air-sea fluxes comprise atmospheric deposition (Atm. Depos.), N-fixation (N-Fix.), and gas exchange (e.g., CO_2). At the sediment-water interface, particulate deposition (Sed. Dep.) and diffusive fluxes (Sed. Dif.) of dissolved inorganic species originating from benthic mineralization and dissolution take place. The bidirectional exchange at the shelf-open ocean interface (Exch. Open Oc.) is simulated dynamically in the model. Nutrients (NUT) consist of dissolved inorganic phosphorus (DIP), dissolved inorganic nitrogen (DIN), dissolved silica (DSi), and dissolved iron (DFe). PHY, ZOO, POM, and mDOM are simulated marine phytoplankton, zooplankton, and combined marine, and terrestrial particulate organic matter and dissolved organic matter species, respectively. (b) Idealized representation of water in- and outflows on continental shelves to estimate residence times of shelf waters of the model. Q_{out} is the water outflow of a continental shelf of volume V_c, Q_{FW} is the freshwater inflow and Q_{OC} is the inflow of open ocean waters. GOBM, Global Ocean Biogeochemical Model; mDOM, marine dissolved organic material pool; POM, particulate organic matter.

the lifetime and death of both phytoplankton and zooplankton. This organic material can be remineralized to dissolved inorganic carbon (DIC) and nutrients via grazers feeding on phytoplankton, or upon the death of the grazers and phytoplankton. Organic matter is remineralized aerobically, while POM can undergo degradation via denitrification and sulfate reduction under anaerobic conditions. Phytoplankton and zooplankton produce opal (PSi) at high DSi concentrations, and $CaCO_3$ shells at low DSi concentrations. Atmospheric dust, which contains Fe, and N deposition are represented and quantified as described by Mauritsen et al. (2019). The DIC speciation is represented in the model based on the inorganic chemistry

formulations of Maier-Reimer and Hasselmann (1987), to which adjustments in the chemical constants according to the Ocean Model Intercomparison Project (Orr et al., 2017) were made (Mauritsen et al., 2019). The model furthermore simulates the gas-exchange fluxes of CO_2, O_2, and N_2 at the air-sea interface.

An advantage of HAMOCC in the context of representing the close linkage of benthic-pelagic processes on the shallow continental shelves is the representation of 12 sediment layers with increasing thickness and decreasing porosity from top to bottom (Heinze & Maier-Reimer, 1999). Particulate deposition fluxes of POM, PSi, $CaCO_3$, and dust from the water column add matter to the top sediment layer, whereas mineralization and dissolution within the sediment release DIC, alkalinity (Alk), and inorganic nutrient species into the sediment pore water. In the deepest sediment layer, a flux to a diagenetically consolidated burial layer is applied to represent the permanent oceanic loss of particulate compounds.

2.3. Model Extensions and Modifications

2.3.1. Representation of Riverine Loads

Oceanic inputs of riverine compounds were prescribed as described in Lacroix et al. (2020). The developed scheme considers DIC, Alk, DIP, DIN, DSi, DFe, tDOM, POM, and Fe-P loads to the ocean. The approach derives both weathering and nonweathering sources of nutrients and carbon, and parametrizes their transformations to organic matter (tDOM and POM) through the global river network using a hierarchy of weathering and terrestrial export models. In the present study, tDOM exports were scaled to an improved global estimate of ~0.24 $TgCyr^{-1}$ by Cai (2011) and Aarnos et al. (2018), resulting in global riverine carbon inputs now representing 0.74 $PgCyr^{-1}$, which is in agreement with the range of global riverine carbon inputs of 0.69–0.78 published by Meybeck and Vörösmaty (1999) and Resplandy et al. (2018). A detailed description of the riverine loads and their comparisons to previous global and regional load estimates can be found in Supporting Information S2 and in Lacroix et al. (2020). We note that riverine POM was added to the oceanic pool of POM, due to the lack of observational constraints to quantify the dynamics of terrestrially derived POM in the ocean, whereas tDOM was characterized as its own model compound pool.

2.3.2. Enhanced POM Mineralization in Shelf Sediments

Although highly variable at regional scales, the remineralization of organic matter in the sediments of continental shelves has been suggested to be more efficient than in deep ocean sediments (Arndt et al., 2013; Giraud et al., 2008; Johnson et al., 1999). This is argued to be mainly due to the comparatively younger age of coastal POM, implying an efficient recycling of carbon and nutrients and a higher importance of benthic remineralization processes in coastal regions compared to the open ocean (Arndt et al., 2013; Johnson et al., 1999). In the study of Pätsch et al. (2018), in which HAMOCC was used in a regional setup for the North Sea, it was indeed concluded that a higher coastal sedimentary POM degradation rate constant than that of the open ocean (e.g., 0.001 $days^{-1}$ used in Mauritsen et al., 2019) was needed to achieve a plausible representation of the biogeochemical features in the region. We therefore tested sedimentary POM degradation rate constants that were 30%–400% higher (0.0013, 0.0026, and 0.0075 $days^{-1}$) for coastal sediments (<250 m depth) than for deep ocean sediments (Supporting Information S3), a range which also should partly account for physical resuspension of organic matter in coastal seas (Mathis et al., 2019). We retained the value of 0.0026 $days^{-1}$ for the rate constant in the main preindustrial simulation, as it provides organic matter burial fluxes that are in broad agreement with published estimates (Krumins et al., 2013) and an improved representation of the coastal biological productivity with respect to the SeaWiFs observation-based product (Behrenfeld et al., 2001). In deep ocean sediments, the remineralization rate constant was kept as 0.001 $days^{-1}$.

2.3.3. tDOM Dynamics in the Ocean

The tDOM pool was represented as a separate model variable since it is acknowledged to already be strongly degraded upon its delivery to the ocean (Ittekkot, 1988; Vodacek et al., 2003) and to have substantially higher C:N and C:P ratios than mDOM (Aarnos et al., 2018; Meybeck, 1982; Seitzinger et al., 2010). Assuming a C:N:P ratio described in the Supporting Information S2.2 and in Lacroix et al. (2020), and a typical organic matter C:H:O ratio (Krumins et al., 2013), the stoichiometric equation for the degradation of tDOM ($((CH_2O)_{2583}(NH_3)_{16}(H_3PO_4))$ in the model reads (ignoring Fe here for conciseness):

$$\left(CH_2O\right)_{2583}\left(NH_3\right)_{16}\left(H_3PO_4\right) + 2615\,O_2 = 2583\,CO_2 + 16\,NO_3^- + H_2PO_4^- + 17\,H^+ + 2599\,H_2O. \quad (1)$$

We performed five simulations to assess the sensitivity of the oceanic distribution and regional budgets of tDOM to the chosen degradation rate constants, including a scenario accounting for a simplified representation of the tDOM photodegradation pathway (Supporting Information S3). These simulations were evaluated against contributions of tDOM to total DOM concentrations in open ocean basins (Benner et al., 2005; Hernes & Benner, 2002; Opsahl & Benner, 1997) and regional tDOM degradation rates derived from budgets or field measurements (Aarnos et al., 2018; Fichot & Benner, 2014; Kaiser et al., 2017). While including a photo-oxidation scheme might improve the representation of seasonality of tDOM degradation on the shelf (Supporting Information S3), we used the simpler first-order degradation scheme for the main simulations, since it yielded similar annual mean surface ocean tDOM concentrations, while avoiding computational expenses of simulating an increased number of advected species in comparison to the photo-oxidation scheme.

2.4. Key Metrics of Physical and Biogeochemical Features of Continental Shelves

2.4.1. Global Continental Shelf Definition

Continental shelves were defined as all ocean model grid cells located in proximity to land for which depths were less than 250 m. The model bathymetry, which is based on the ETOPO2 bathymetry (US Department of Commerce and Atmospheric Administration, 2006), was used to delineate continental shelves at depths of less than 250 m. The 250 m threshold chosen here is slightly more inclusive than the 200 m cut-off depth usually used to delineate the global continental shelf (Chen & Borges, 2009; Laruelle et al., 2013, 2010 and citations therein). We used 250 m for a better areal representation of the global shelf in our still relatively coarse spatial setup when considering the fine scales of the coastal ocean. The global NEP and FCO_2 over continental shelves were, however, also computed using isobaths of 50, 150, 250, 400, and 1,000 m to delineate the shelf limit. We also excluded Antarctic shelves ($\sim 2 \times 10^6$ km^2 using the 250 m depth threshold) from our analysis of the continental shelf carbon budgets due to their markedly different characteristics compared to other shelves (deeper depths, extensive ice coverage, and limited riverine loads).

Our continental shelf definition covers a total surface area of 24.5×10^6 km^2, which corresponds to ~7% of the global ocean surface. This surface area is at the low end of previously reported estimates of global shelf areas, which range from 22 to 30×10^6 km^2 (Borges et al., 2005; Cai, 2011; Chen & Borges, 2009; Laruelle et al., 2013, 2010; Walsh, 1988). In Laruelle et al. (2013), using a 200 m depth cut-off yielded a surface area of 26.39×10^6 km^2 (including Antarctic shelves). The volume of the global shelf is 1.78×10^6 km^3, which compares well with the value of 1.79×10^6 km^3 given in Laruelle et al. (2013) for their 250 m delineation.

We defined 13 shelf regions for which we quantified hydrodynamical and biogeochemical features: Laptev Sea, Beaufort Sea, Barents Sea, Sea of Okhotsk, North Sea, Eastern North America, South Atlantic Blight, East China Sea, Bay of Bengal, Sunda Shelf, Tropical West Atlantic, Great Barrier Reef, and Patagonia (see Supporting Information S1 for their delineations). These regions were chosen due to being extensive, and also due to the availability of data to validate the model in these regions. In addition, we also defined three river plume areas (Amazon, Congo, Ganges), which were chosen to delineate areas of large salinity gradients caused by large river outflows in the model.

2.4.2. Physical Indicators: Water RTs and Mixed Layer Depths

We implemented a dye tracer in the ocean model to estimate water RTs on the global shelf. This tracer was initially added in each grid cell proportionally to their volumes, and once it was exported beyond the shelf break, the tracer value was set to nil. We performed simulations including the tracer in all shelf waters (ASWs), in surface waters (SWs) only, using the first model vertical layer of 10 m depth on average, as well as a simulation adding the tracer solely in areas where the surface salinity was one standard deviation (1.9 PSU) less than the global mean surface salinity (34.6 PSU) as a surrogate for riverine freshwater (FW) plumes.

We approximated RTs by applying simple first-order kinetics for the loss of the inert tracer mass (M) on the shelf, which also corresponds to the export of M off a shelf with a volume V_c (Figure 1b, also as described in Monsen et al., 2002):

$$\frac{dM}{dt} = \frac{Q_{out}}{V_C} * M(t) \tag{1}$$

This approximation assumes a well-mixed shelf in the vertical, and outflows across the shelf break to be much larger than their variations in time (i.e., their seasonality). Furthermore, it is only valid if water exports off the shelf are substantially larger than their exchange within the shelf. While these assumptions introduce a certain degree of uncertainty when comparing modeled shelf water RTs against observations, it is important to stress that they do not affect the actual exchange of water and of biogeochemical compounds, since these exchanges are computed dynamically in our 3D-coupled MPI-OM-HAMOCC model.

The ratio Q_{out}/V_c defines the time constant k_{exp} for an exponential decay of the dye tracer, for which we computed means and 95% confidence intervals at regional and global scales using the MATLAB curve fitting tool *cftool*. The RTs were then calculated from the spatially mean exponential decay constants according to:

$$RT = \frac{1}{k_{exp}} \tag{2}$$

Q_{out} is also equal to the sum of freshwater inputs Q_{FW} and oceanic inflows Q_{OC}. Oceanic inflows can therefore be approximated through:

$$Q_{OC} = \frac{V_C}{RT} - Q_{FW} \tag{3}$$

The mixed layer depths (MLDs) of continental shelf waters, which we use to provide an indication of the degree of stratification within the water column, were computed by the MPI-OM according to the Coupled Model Intercomparison Project Phase 6 protocol (Griffies et al., 2016). They are therein defined as the depths, at which the water density deviates by 0.03 kg m^{-3} from the surface layer.

2.5. Biogeochemical Indicators: NEP and Cross-Shelf Exports

The NEP (GPP-NER) represents the net interconversion of carbon between DIC and organic matter pools. In HAMOCC, the net primary production (NPP) is directly computed by the model, which already implicitly accounts for the GPP and the autotrophic respiration of the phytoplankton. The NEP was thus calculated as the simulated NPP of phytoplankton and cyanobacteria minus the simulated heterotrophic degradation of organic matter (RH), which consists of the pelagic mineralization of tDOM and mDOM, grazing and respiration of ZOO, and the pelagic and benthic mineralization of POM:

$$NEP = NPP - RH$$

Finally, the net cross-shelf export resulting from the difference between exports from the shelves and supplies from open ocean inflows was calculated through the closure of the continental shelf budget, considering all sources and sinks for each tracer, as well as their change in inventory. The source fluxes of organic matter are thereby riverine inputs and NPP, whereas its sinks comprise RH and sediment deposition. Source fluxes of DIC originate from riverine inputs and RH, whereas both NPP and net $CaCO_3$ production lead to sinks of DIC, with the FCO_2 being either a further sink or a source.

3. Results and Discussion

In this section, we begin by first assessing the continental shelf RTs of our model, which are central drivers for biogeochemical transformations in these shallow waters. This analysis is valid for both preindustrial and contemporary time periods since the physical climate forcing is not altered in our transient simulation. We then compare the simulated biogeochemical metrics to relevant present-day observation-based estimates

and their distributions, and, finally, we travel back in modeled time to revisit carbon fluxes on continental shelves at preindustrial conditions.

3.1. Continental Shelf Water RTs

The RT of continental shelf waters is an important property as it determines the timescale at which biogeochemical transformation processes can occur on the shelves. Since the model resolution used here is relatively coarse with respect to regionally focused modeling approaches (Fennel & Wilkin, 2009; Frischknecht et al., 2018; Gruber et al., 2011; Mathis et al., 2019), which might limit the representation of the physical and biogeochemical dynamics in the coastal ocean (Mathis et al., 2018), it is important to evaluate the extent to which our model plausibly reproduces shelf RTs at the global scale and whether realistic exposure times of biogeochemical compounds to transformations on the shelf can be inferred from our simulations.

The simulated evolution of the dye tracer mass residing on the shelf reveals that half of the global shelf water is transported offshore within 4 months for ASWs and for SWs, whereas this takes less than 3 months for FW (Figures 2a–2c). Our assumption of an exponential loss of the inert dye mass off the shelf holds reasonably well at the global scale, although we observe a faster initial loss for ASWs and for SWs than the fitted exponential function during the first 8 months, and a slower loss rate thereafter. The faster initial loss rate of ASWs and SWs than predicted by the exponential decay function is possibly caused by the rapid export of shelf FW (as seen in Figure 2c), whereas the slower loss rate after 8 months is possibly a consequence of shelf water being trapped in semi-enclosed basins with limited exchange with the open ocean, such as in the Hudson Bay or the Baltic Sea. Because heterogeneity decreases with the spatial scale of the coastal system under investigation, the assumption of an exponential decay for the decrease of the tracer mass on the shelf holds better for individual regions than at global scale (Figures 2d–2o), following the conceptual view depicted in Figure 1b. Seasonal effects on the exports of shelf water are also noticeable in regions for which the mean annual water exports from the shelf are noticeably low in relation to the region's shelf volume, as in the Laptev Sea and on the Patagonian Shelf (Figures 2d and 2l).

Using estimated 95% confidence interval for the k_{exp} values of the exponential decay function, we approximate global RTs of 12–17 months for ASWs and SWs, and of 3–4 months for FW. At the regional scale, our simulations reveal large spatial variability of continental shelf water RTs (Figure 3a), which, at first order, agree reasonably well with those reported in the parameterized approach of Sharples et al. (2017) (Figure 3b), with the global high-resolution model estimates of Liu et al. (2019) (Table 1), as well as with published estimates from field measurements or regional models (Table 1). Our results are also supportive of the conclusions by Liu et al. (2019), which found that the shelf geometry is a major driver of shelf water RTs. For instance, the shallow and narrow shelves of the Great Barrier Reef, the South Atlantic Bight, the tropical West Atlantic and the Bay of Bengal are simulated to have particularly low shelf water RTs (<2 months) in our study and in Liu et al. (2019). In contrast, many wide Arctic shelves exhibit much longer RTs (>2 years) than average. A stronger Coriolis force at higher latitudes could also help explain the longer simulated RTs in the region, since it deviates the flow of river plumes and coastal currents, thereby reducing cross-shelf outflows and increasing retention on the shelf in these regions (Sharples et al., 2017). RTs have also been reported to vary within large regions such as for the Canadian Shelf, where an observation-based study of Rutherford and Fennel (2018) reports relatively short RTs in the Grand Banks area (3 months on average), whereas the Gulf of Maine, Scotian Bay (around 6 months each) and, to an even larger the degree, the Gulf of St. Lawrence (12 months on average) have longer RTs. The same pattern emerges from our model although RTs are somewhat overestimated compared to observations, with values of 3, 5–9, 9, and 24 months for these subregions, respectively (Figure 3a).

In past investigations of carbon cycling on continental shelves, conceptual box model studies have assumed global shelf RTs from 4 years to a decade (Andersson et al., 2005; Mackenzie et al., 2004; Rabouille et al., 2001), which is significantly longer than the global RT estimated here and than typical regional RTs reported by Liu et al. (2019, Table 1). The long RTs assumed in box models were constrained from estimates of global shelf volume, freshwater inflows and, if considered, open ocean inflows derived largely from upwelling regions. This approach would yield RTs of several decades, as already shown by Laruelle et al. (2013). Our much lower global estimate derived from a 3D resolving model suggests that inflows from the open ocean play a prominent role in the quantification of shelf RTs and that they were systematically

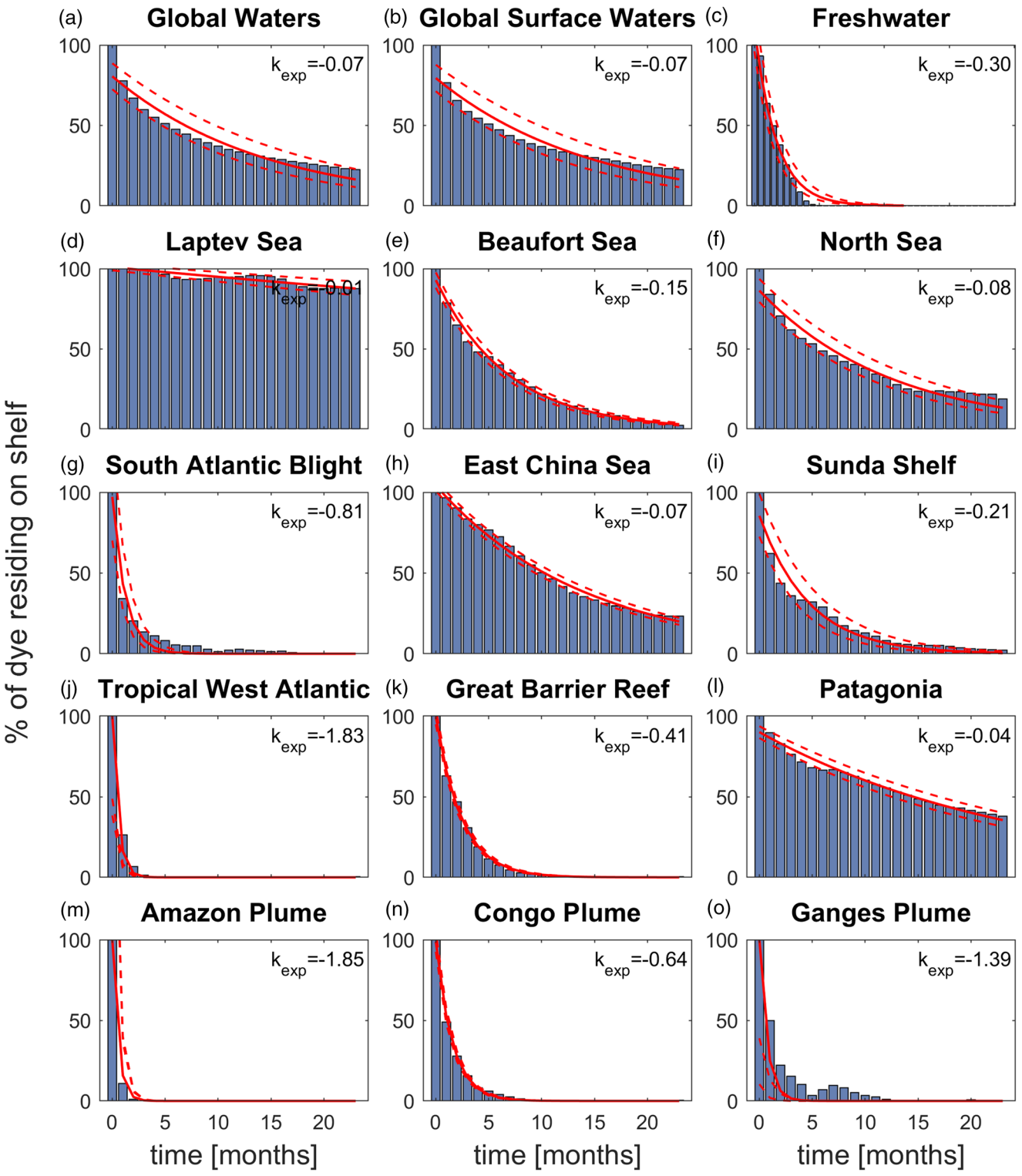

Figure 2. Percentage (%) of inert dye mass remaining on the shelves after its initial injection for (a) all global shelf waters (ASWs), (b) global shelf surface waters only (SWs), (c) riverine freshwater (FW), and for the (d) Laptev Sea, (e) Beaufort Sea, (f) North Sea, (g) South Atlantic Bight, (h) East China Sea, (i) Sunda Shelf, (j) Tropical West Atlantic, (k) Great Barrier Reef, (l) Patagonia. Values are also reported for the freshwater plumes of the (m) Amazon, (n) Congo, and (o) Ganges rivers. The fitted means (red full line) and 95% confidence intervals (red dotted line) as well k_{exp} values (months^{-1}) are shown. See Supporting Information S6 for the complete listing of time constants.

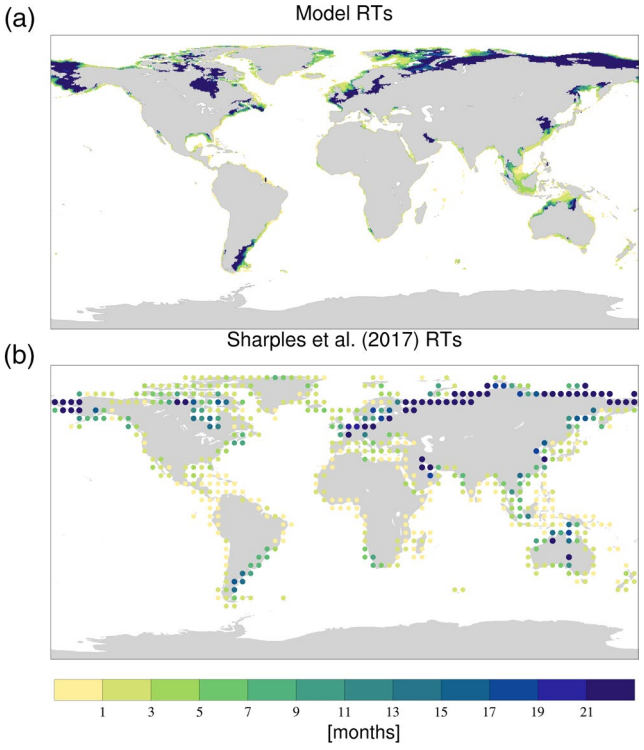

Figure 3. Continental shelf surface water residence times (RTs; in months) derived from (a) the near-exponential decay of the simulated inert tracer mass for all shelf waters and (b) RT data points computed by the parameterized approach of Sharples et al. (2017) to quantify river plume RTs on the shelves.

underestimated in the mentioned box model approaches. On average, our simulations reveal that global open ocean inflows are about 40 times larger than global freshwater inputs by contrasting modeled freshwater inputs of 32×10^3 km^3 yr^{-1} (global estimate of 39×10^3 km^3 yr^{-1} by Fekete et al., 2002), and our global estimate of open ocean inflows (1.4×10^6 km^3 yr^{-1}; Table 1).

Our analysis furthermore shows that open ocean inflows are larger than the freshwater inputs in all investigated regions except for the Laptev Sea. In the North Sea, for instance, the simulated open ocean inflows of 52.3×10^3 km^3 yr^{-1} are over 50 times larger than freshwater inputs of 0.8×10^3 km^3 yr^{-1} to the region, with both values showing good agreement with regional estimates of around 50×10^3 and 0.3×10^3 km^3 yr^{-1}, respectively (Mathis et al., 2013; Thomas et al., 2005). In the East China Sea, the simulated open ocean inflows of 269×10^3km^3 yr^{-1} are also much larger than the simulated freshwater inputs of 1.0×10^3 km^3 yr^{-1}, which is supported by open ocean inflows of 598×10^3 km^3 yr^{-1} and freshwater inputs of 0.9 10^3 km^3 yr^{-1} computed by the high-resolution model of Zhou et al. (2015). The lower cross-shelf export simulated in the East China Sea is also reflected by the slightly higher regional RT than is estimated in other studies (Table 1), with complex fine-scale circulation structures sketched in Zhou et al. (2015) likely only being coarsely represented by our model. The dominance of open ocean inflows is even revealed in the Tropical West Atlantic and the Bay of Bengal (Table 1), which are notable regions of large riverine inputs. Within these regions however, the Amazon and the Ganges plumes (Figures 2m and 2o) exhibit noticeably shorter RTs than their corresponding shelf regions, which, along with strong stratification (mean MLDs of 16 and 8.7 m, respectively), favor an efficient cross-shelf export of freshwater. This effect caused by the dynamics of river plumes has already suggested by Sharples et al. (2017) for plumes wider than their respective shelf widths. Therefore, while major riverine freshwater inflows may strongly impact the RTs locally, our simulations suggest that inflows from the open ocean are generally the dominant control of all the regional shelf water RTs analyzed in this study. As a result of the minor importance of freshwater for shelf RTs at the global scale, the computed RTs from the SW and ASW simulations are practically indistinguishable.

The dominance of oceanic inflows determined here have important potential implications for the biogeochemical dynamics on continental shelves. In addition to their profound effects on shelf RTs and physical properties within the water column, the chemical composition of these waters likely differs markedly from the land-derived riverine inflows. The significantly shorter RTs of FWs on the shelves, and the even shorter RT of the individual plumes, however, still acts as an important control factor for the fate of terrestrially derived carbon and nutrients on the shelves. By favoring an efficient export of material to the open ocean, short FW RTs limit the imprint of land-derived inputs on the shelf carbon cycling at the global scale and further reinforce the influence of the inflows from the open ocean.

Regional-scale RT studies show strongly varying estimates for the same regions, and large uncertainties are reported within individual studies, especially in in situ tracer studies (Table 1). Our results are consistent with these large ranges, but nevertheless still do not provide a perfect representation of the coastal ocean because of the relatively coarse model resolution used here. In addition, the exposure time of biogeochemical compounds could be affected by vertical and horizontal fine-scale heterogeneities in the coastal ocean that might not be accounted for in our simulations. We, however, do not observe a systematic positive or negative bias, as was previously suggested for global models based on a regional-scale study for the Canadian Shelf (Rutherford & Fennel, 2018), when comparing our simulated RTs with observational studies and higher resolution model runs (Table 1). It is, therefore, more likely that a complex interplay of fine-scale effects that vary in importance between regions needs to be advocated to explain the influence of our model's spatial resolution on the shelf hydrodynamics.

Table 1
*Estimated k_{exp} ($mths^{-1}$: $months^{-1}$) and Continental Shelf RTs (mths) Derived From the Near-Exponential Decay of Our Simulated Inert Tracer Mass (**RT Mod.**), Compared to Regional Estimates Obtained From a Combination of In Situ Tracer Experiments and High-Resolution Regional Models (**RT obs.**), and Globally Simulated RTs at a 0.1° Resolution in Liu et al. (2019) for the Regions Closest to Our Definitions (**RT HR**). In addition, the model shelf volume Vc, the estimated total inflows Qin, the model freshwater inflows QFW, the estimated oceanic inflows Qoc, the simulated mixed layer depth (MLD) and model Sea Floor Depth (SFD) for each region are given. RT, residence time.*

Global / Regions /*Plumes*	k_{exp}	RT Mod.	RT obs.	RT HR	V_c	Q_{in}	Q_{FW}	Q_{oc}	MLD	SFD
	($mths^{-1}$)	(mths)	(mths)	(mths)	[10^3 km^3]	(10^3 km^3 yr^{-1})	(10^3 km^3 yr^{-1})	(10^3 km^3 yr^{-1})	(m)	(m)
All shelf waters	*0.07*	*14.5*	–	–	*1.780*	*1,473*	*32*	*1,442*	*37*	*92*
Shelf surface waters	*0.07*	*14.5*	–	–	*312*	*258*	*32*	*226*	–	–
Freshwater	*0.29*	*3.4*	–	–	–	–	–	–	–	–
Laptev Sea	0.01	163.9	12–72[a]	56	11	0.8	0.7	0.1	13	31
Beaufort Sea	0.01	71.4	–	11	9	1.5		1.5	16	90
Sea of Okhotsk	0.06	16.7	9–48[a]	10	4	3.0	0.3	2.6	52	153
North Sea	0.08	12.3	5–48[b]	21	54	52.3	0.8	51.5	41	71
South Atlantic Bight	0.81	1.2	1[c]	1	9	90.5	0.1	90.4	27	61
East China Sea	0.07	13.9	6–48[d]	7	53	270.4	1.0	269.3	29	63
Bay of Bengal	0.49	2.0	3[e]	3	12	67.6	1.8	65.8	16	68
Sunda Shelf	0.21	4.8	1–12[f]	6	164	413.3	0.1	413.2	24	65
Tropical West Atlantic	1.83	0.5	0.5–1[g]	1	9	197.6	6.8	190.8	15	61
Great Barrier Reef	0.41	2.4	0.5–2[h]	2	14	67.4	0.7	66.7	36	80
Patagonia	0.04	24.4	–	19	86	42.3	0.1	42.2	52	109
Amazon Plume	*1.85*	*0.5*	–	–	*0.8*	*17.8*	*0.1*	*17.6*	*11*	*26*
Congo Plume	*0.64*	*1.6*	–	–	*2.7*	*20.7*	*0.1*	*20.6*	*7*	*120*
Ganges Plume	*1.39*	*0.7*	–	–	*0.3*	*5.0*	*0.1*	*4.9*	*9*	*45*

[a]Schlosser et al. (1994), Eicken et al. (2005). [b]Yamamoto et al. (2001), Yasuda et al. (2002). [c]Huthnance (1997), Blaas et al. (2001). [d]Gong et al. 2010. [e]Nozaki et al. (1989), Ren et al. (2006), Men and Liu (2015). [f]Sarin et al. (1994). [g]Mayer et al. (2015). [h]Moore and de Oliveira (2008). [i]Hancock et al. 2006.

3.2. Present-Day Oceanic Carbon Cycling at the Global Scale

In order to compare our simulation to observation-based datasets, we use the 1998–2015 period of our transient simulation. The simulated global mean NPP value of ~47 $PgCyr^{-1}$ for this time period compares well to satellite-based estimates of 50 ± 10 $PgCyr^{-1}$ (Behrenfeld et al., 2001; Carr et al., 2006) and to previous GOBM studies (e.g., ~46 $PgCyr^{-1}$ in Paulsen et al., 2017). The export production at 90 m is 6.2 $PgCyr^{-1}$, implying a vertical POM export efficiency of 13% from the approximated euphotic zone. Although large uncertainties are associated with the magnitude of the vertical POM export from the euphotic zone, previous studies report values ranging from 4 to 12 $PgCyr^{-1}$ (DeVries & Weber, 2017; Henson et al, 2011). The simulated pelagic $CaCO_3$ production and export (0.66 and 0.21 $PgCyr^{-1}$, respectively) are also comparable to the values reported by Milliman and Droxler (1996) (>0.49 and 0.25 $PgCyr^{-1}$), which were obtained from upscaling observational data points. Overall, this implies that the model agrees with previously reported POM and $CaCO_3$ production and export estimates at the global scale, albeit all values presented here are associated with a high degree of uncertainty.

The simulated global present-day atmospheric CO_2 uptake of 1.8 $PgCyr^{-1}$ implies that the ocean is a sink of 2.1 $PgCyr^{-1}$ of anthropogenic carbon in the model, given that we simulate a preindustrial oceanic carbon outgassing flux of 0.32 $PgCyr^{-1}$. These values are consistent with estimates for the present-day anthropogenic sink (2.6 ± 0.6 $PgCyr^{-1}$; Friedlingstein et al., 2020), and for the preindustrial carbon source to the atmosphere (0.2–0.8 $PgCyr^{-1}$; Jacobson et al., 2007; Lacroix et al., 2020; Resplandy et al., 2018; Sarmiento & Sundquist, 1992).

The simulated surface nutrient concentrations of DIP and DIN are slightly underestimated in comparison to the observational data set of the World Ocean Atlas 2013 (WOA; 0.36 μM DIP simulated compared to

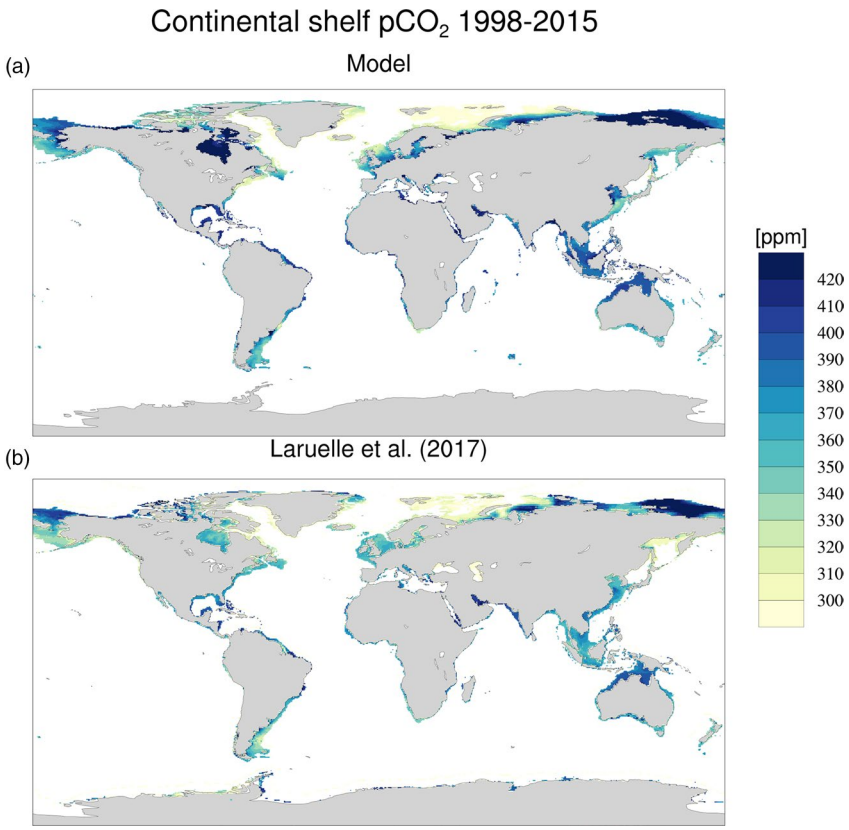

Figure 4. Annual mean pCO_2 fields (ppm) over continental shelves for 1998–2015 (a) modeled in this study (model) and (b) derived from a neural network-based interpolation of observational data (Laruelle et al., 2017). Out of consistency, Laruelle et al. (2017) data points are only shown for depths shallower than 250 m.

0.47 μM DIP from the WOA, 4.4 μM DIN simulated compared to 5.1 μM DIN) and overestimated for DSi (13.7 μM Si simulated compared to 9.9 μM Si in WOA). These biases and their distributions are similar to previous model versions (e.g., Lacroix et al., 2020; Paulsen et al., 2017; Supporting Information S5). The overestimation of DSi is however unlikely to affect the results presented here since the globally averaged bias largely originates from the Southern Ocean, an oceanic region poorly represented in state-of-the-art GOBMs (Meijers, 2014).

The simulated continental shelf NPP (2.95 $PgCyr^{-1}$) contributes to around 6% of the global NPP, which is below the 10%–30% range reported until now (Gattuso et al., 1998; Mueller-Karger et al., 2005; S. V. Smith & Hollibaugh, 1993) from satellite products, which comprise large uncertainties in coastal areas (Saba et al., 2011), and the upscaling of limited observational data. Our transient simulation, however, excludes the substantial increase in riverine nutrient inputs over the 20th century (Beusen et al., 2016), which has been reported to cause significant NPP increases in a multitude of coastal regions (Fennel & Testa, 2019), as well as the explicit representation of resuspension of nutrients from the sediment (as modeled in Mathis et al., 2019), which could explain part of the discrepancy. The deposition flux of POM on the shelf seafloor (0.52 $PgCyr^{-1}$) accounts for two-thirds of the global sedimentary deposition (0.79 $PgCyr^{-1}$). This proportion is in line with earlier estimates derived from upscaling of field measurements, which suggest that continental shelves are hotpots of organic carbon deposition (Chen & Borges, 2009; Gattuso et al., 1998; S. V. Smith & Hollibaugh, 1993). The continental shelf organic burial efficiency of around 21% (organic matter burial, 0.11 $PgCyr^{-1}$, to POM deposition ratio) also compares well with the range of 8%–41% (net burial of 0.06–0.67 $PgCyr^{-1}$) reported in a review by Krumins et al. (2013).

The spatial variability of the present-day continental shelf pCO_2 simulated by our model is in good agreement with the interpolation-based data set of Laruelle et al. (2017) (Figure 4). The simulated model distributions show a pCO_2 underestimation off the eastern North American and Canadian shelves, which might

be driven by circulation biases of our relatively coarse model in these regions (Rutherford & Fennel, 2018). Overestimations on the Sunda Shelf are likely of biogeochemical nature, since coral reefs present in the region are not represented in the model, while bias in the Arctic are likely due to the complexity of representing sea-ice dynamics in ocean models. Our model also exhibits a positive pCO_2 bias in most semi-enclosed seas for which geometry cannot be reproduced accurately by our model at its current resolution. Increases in riverine nutrient supplies during the 20th century, which are not accounted for in this study, also might help explain the discrepancy between our modeled present-day pCO_2 and that of Laruelle et al. (2017) in certain near-shore areas. In regions such as the North Sea, Louisiana Shelf, and Southeast Asia, riverine nutrient exports have increased substantially since the 1950s (Rabalais et al., 2002; Radach & Pätsch, 2007; Wang et al., 2015), which could reduce the pCO_2 through the enhancement of the biological carbon uptake. Overall, our simulated mean global pCO_2 is higher than that of Laruelle et al. (2017), which suggests that the global continental shelf has a small bias toward outgassing in the model. This slight bias toward outgassing is also confirmed by comparing our simulated CO_2 uptake of 0.15 $PgCyr^{-1}$ on the global continental shelf with the reported range of 0.14–0.25 $PgCyr^{-1}$ (Laruelle et al., 2014; Roobaert et al., 2019; Wanninkhof et al., 2013) for the present day.

The model indicates a strong CO_2 sink at temperate latitudes (0.08 and 0.02 $PgCyr^{-1}$ for 30°–60° of the Northern and Southern Hemispheres, respectively), a sink over the entire Arctic (0.04 $PgCyr^{-1}$ for over 60°N) and a weak source at subtropical and tropical latitudes (<0.01 and <0.01 $PgCyr^{-1}$ at 0°–30° for the Northern and Southern Hemispheres, respectively). This compares roughly to previous latitudinal budgets (Laruelle et al., 2010; Roobaert et al., 2019), as well as to compiled regional budgets (Chen & Borges, 2009; Fennel et al., 2019; Thomas et al., 2005; see Table S7). Even within regions, however, strong longitudinal variability in pCO_2 can be observed in our simulation as well as in the data set of Laruelle et al. (2017). For instance, the Barents Sea is characterized by very low pCO_2 levels (<300 μatm locally), while the Laptev shelf located at similar latitudes shows some of the highest pCO_2 values globally (>450 μatm locally), with both of these findings being corroborated by recent observational studies (Anderson et al., 2009; Lauvset et al., 2013; Pipko et al., 2017; Semiletov et al., 2013).

3.3. Preindustrial Organic Carbon Cycling on Continental Shelves

The key transport and transformation fluxes of the preindustrial organic carbon cycle (Figure 5a) are nearly identical to those reported in the previous section for the present day, which is expected, since the increasing atmospheric pCO_2 is the only driver of change in our transient simulation. The net sources of organic carbon to continental shelf waters comprise riverine tDOM (0.24 $PgCyr^{-1}$) and POM inputs (0.11 $PgCyr^{-1}$), as well as 2.95 $PgCyr^{-1}$ of organic matter production (mDOM + POM) via NPP (Figure 5a F1, F2, and F3, respectively). Our model quantifies that around three-quarters (2.21 $PgCyr^{-1}$) of the mDOM and POM stocks, and about half (0.12 $PgCyr^{-1}$) of the tDOM stock is mineralized in global shelf waters (F6 and F5, respectively), excluding their degradation in the sediment. We note that POM values reported here comprise both terrestrial and marine POM, since their dynamics are simulated within the same model pool. We also estimate that out of the 0.52 $PgCyr^{-1}$ POM flux deposited on shelf sediments (F4), roughly 80% (0.41 $PgCyr^{-1}$) is recycled back to the water column via benthic mineralization (F7), while the remainder is lost through burial (0.11 $PgCyr^{-1}$, F8). The budget of organic carbon sources and sinks occurring within the shelf aquatic-sediment continuum thus implies that the global shelf NEP is positive ($F3 - F5 - F6 - F7 = 0.20$ $PgCyr^{-1}$), meaning that the organic carbon cycling on the shelf causes a DIC sink. This autotrophic state is consistent with the simulated efficient export of terrestrial and marine organic matter across the shelf break globally ($F9 + F10 = 0.44$ $PgCyr^{-1}$), indicating that a considerable amount of both autochthonous and allochthonous organic matter is exported offshore before it can be degraded on the shelves.

Regionally, the model simulates both areas of strong autotrophy, as well as of strong heterotrophy both on continental shelves (Figure 6a), as well as in the open ocean (Figure 6b). Strongly autotrophic shelf regions are deep and extensive regions, which are also suggested to be heavily influenced by oceanic subsurface inflows in our model (see Section 3.1), as well as in published literature (Patagonian Shelf, Combes & Matano, 2018; Song et al., 2016; the Eastern North American, Fennel et al., 2019; Loder et al., 1993; the East China Sea, Qiao et al., 2006; the outer North Sea shelf, Mathis et al., 2019; Table 1). This occurrence aligns with the conceptual view of Chen and Borges (2009) that entrained nutrients from subsurface open ocean

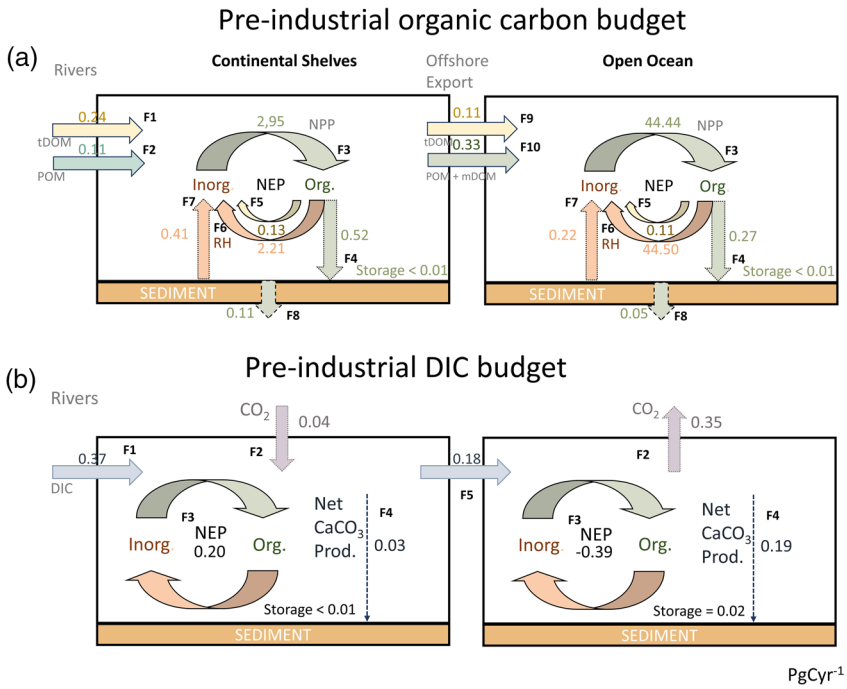

Figure 5. (a) Global annual organic carbon fluxes on continental shelves and in the open ocean under preindustrial conditions ($PgCyr^{-1}$). The reported fluxes are **F1:** Riverine tDOM inputs, **F2:** Riverine POM inputs, **F3:** NPP of phytoplankton and cyanobacteria, **F4:** Sediment deposition of POM, **F5:** Mineralization of tDOM, **F6:** Mineralization of mDOM and POM (both terrestrial and marine), **F7:** Mineralization of POM in the sediment, **F8:** POM burial, **F9:** Offshore export of tDOM calculated from the continental shelf budget as F1 − F5, **F10:** Offshore export of mDOM and POM, calculated from the continental shelf budget as F2 + F3 − F4 − F6. (b) Global preindustrial DIC budget on continental shelves and in the open ocean, including net fluxes from the organic cycling of carbon, as well as inorganic carbon dynamics ($PgCyr^{-1}$). The reported fluxes are **F1:** Riverine DIC inputs to the shelf, **F2:** FCO_2, **F3:** Combined pelagic and benthic NEP, calculated from panel (a) as F3 − F5 − F6 − F7, **F4:** Net $CaCO_3$ production, **F5:** Offshore export of DIC, computed from the continental shelf budget as F1 + F2 − F3 − F4. Storage corresponds to the small accumulations of carbon within the ocean water column as a result of a model drifts. DIC, dissolved inorganic carbon; mDOM, dissolved organic material pool; NEP, net ecosystem productivity; POM, particulate organic matter; tDOM, terrestrial dissolved organic matter.

inflows enhance the shelf NPP, but that the inputs of organic matter originating from these waters do not considerably affect the shelf RH, resulting in net autotrophy in such regions. In contrast, Arctic shelves are largely net heterotroph due to low insolation, long shelf water RTs and substantial organic matter inputs of riverine origin. In addition, large low-latitude shelves with high insolation and high temperature are often areas of positive NEP in the model, whereas regions with large terrestrial organic matter inputs (e.g., the Amazon and Ganges plumes) are net heterotroph.

The substantial offshore transport of organic matter and the resulting positive NEP differ from the results of box model studies (NEPs of 0.1 to −0.3 $PgCyr^{-1}$). This can be explained by the explicit representation of global spatial features and oceanic inflows in our model, which lead to shorter simulated shelf RTs. These short RTs of 14 months on average reduce the timeframe for the degradation of organic matter on the shelf with respect to the assumed RTs of 4 years to a decade in box model approaches. In addition, in our approach, the much lower RTs of major river-borne waters that are induced by plume flows and salinity-induced stratification result in a substantial offshore transport of riverine tDOM. This relatively efficient offshore export is backed up by recent observation-based regional shelf budgets which report that 50%–70% of tDOM is exported offshore in several studied regions (Aarnos et al., 2018; Fichot & Benner, 2014; Kaiser et al., 2017). Our simulated tDOM export off the global shelf (Figure 5 F9), which comprises 47% of the global tDOM riverine input, is consistent with this reported range, and the comparison even suggests that the offshore export of tDOM might be larger, potentially driving the global shelf NEP toward more positive values than simulated here. Despite this broad agreement regarding the fate of tDOM and the model's

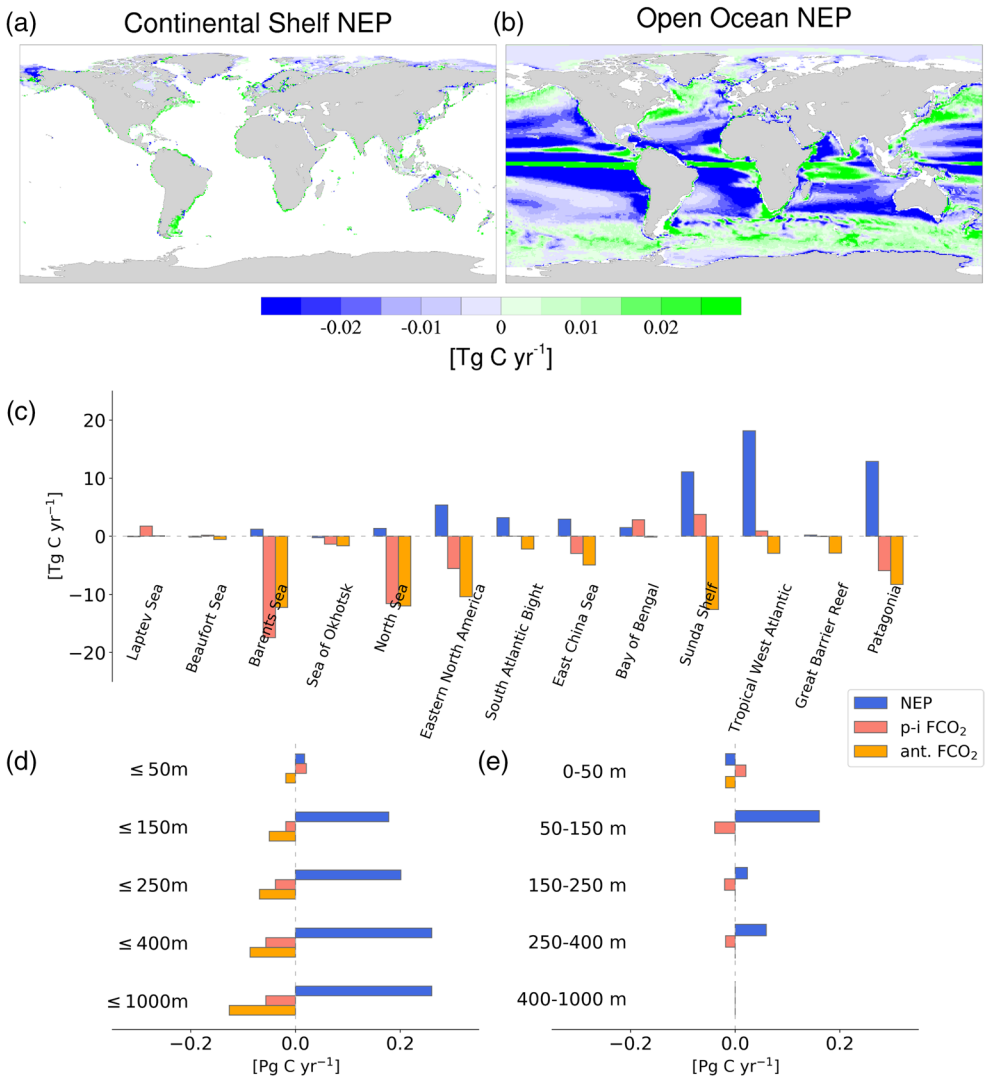

Figure 6. Spatial distribution of the vertically integrated annual NEP ($TgCyr^{-1}$) in (a) the coastal ocean and (b) the open ocean. (c–e) A comparison of NEP, preindustrial FCO_2 (p-i FCO_2) in $PgCyr^{-1}$ and anthropogenic FCO_2 (ant. FCO_2) for 13 chosen regions, for global shelf definitions using of less or equal 50, 150, 250, 400, and 1,000 m sea floor depths and for the intervals between the delineation depths, respectively. The ant. FCO_2 corresponds to the change over the 1800–2015 period calculated by fitting a linear trend to the simulated FCO_2 timeseries and multiplying the trend per year by the total number of simulation years. A positive CO_2 flux represents a flux from ocean to atmosphere. NEP, net ecosystem productivity.

capability to reproduce present-day distributions of key biogeochemical variables, fine-scale circulation features that are not captured by our global simulations introduce significant uncertainties, which may propagate in our assessment of the preindustrial NEP and exports of organic matter off the shelves.

3.4. Preindustrial Continental Shelf FCO_2

At preindustrial model conditions, net DIC sources to the global continental shelf originate from riverine inputs (0.37 $PgCyr^{-1}$, given as F1 in Figure 5b), as well as from a slight uptake of atmospheric CO_2 of 0.04 $PgCyr^{-1}$ (F2). In turn, the net DIC sinks of the global shelf arise from the positive NEP (0.20 $PgCyr^{-1}$, considering both water column and sediment, F3), the net ecosystem calcification (0.03 $PgCyr^{-1}$, $CaCO_3$ production minus dissolution, F4) and the offshore export of DIC to the open ocean (0.18 $PgCyr^{-1}$, F5).

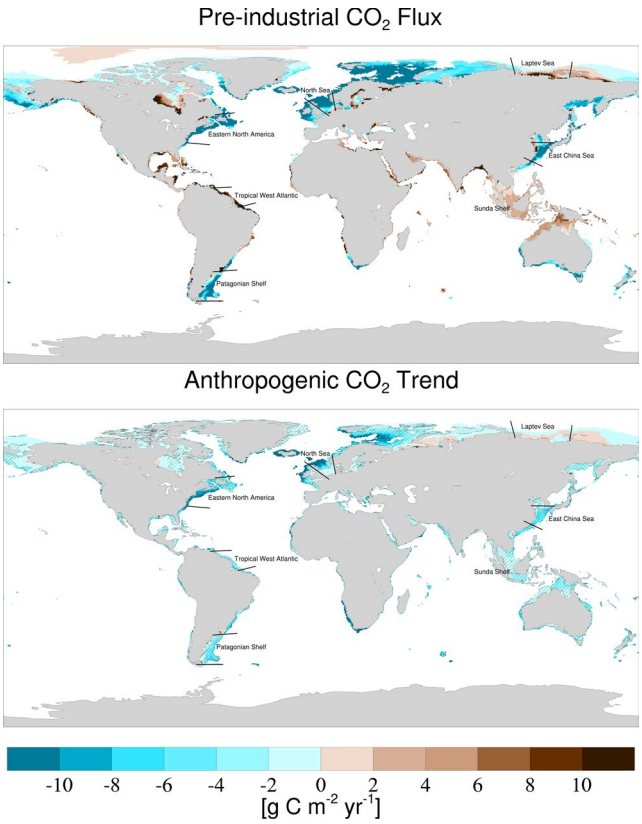

Figure 7. (a) Preindustrial continental shelf air-sea CO_2 exchange (FCO_2), (b) anthropogenic FCO_2 estimated by calculating the FCO_2 trend over the 1800–2015 period and multiplying the trend by the total amount of simulation years. A positive CO_2 flux represents a flux from the ocean to atmosphere. The hatched area represents regions where a significant trend ($p < 0.05$) was computed over the given time period.

The preindustrial CO_2 sink is substantially smaller than the sink of DIC induced by the positive NEP on continental shelves (difference of 0.16 $PgCyr^{-1}$). This underlines that while the positive NEP is certainly an important factor in explaining the simulated CO_2 sink on the global shelf, it is only one of the drivers that affect the shelf CO_2 exchange, as is discussed, for instance, in Thomas et al. (2005). If largely driven by the biological organic matter production and its degradation, the FCO_2 would also closely reflect the NEP in magnitude. This discrepency is due to the FCO_2 depending on circulation, the physical water properties (temperature and salinity), $CaCO_3$ production, and inputs of DIC and Alk from oceanic inflows and riverine sources.

As for the NEP, the sign and magnitude of the simulated preindustrial FCO_2 is spatially variable between different regions (Figures 6c and 7a). The North Sea (11.6 $TgCyr^{-1}$), the East China Sea (5.9 $TgCyr^{-1}$), the eastern North American shelf (5.5 $TgCyr^{-1}$) and the Patagonian shelf (3.0 $TgCyr^{-1}$), which are also deep and extensive shelves of positive NEPs driven by large open ocean inflows, are strong contributors to the preindustrial atmospheric CO_2 sink over the global continental shelf (Figure 6c). They are also strong CO_2 sinks per surface area (Figure 7a). Other regions that we investigated show disagreement in the signs of their regionalized NEP and FCO_2. Preindustrial CO_2 sources can be found on the Sunda shelf (3.73 $TgCyr^{-1}$) and Tropical West Atlantic (0.89 $TgCyr^{-1}$), despite these regions exhibiting positive NEPs (Figure 6c). The carbon source to the atmosphere in these regions is likely caused by the heating of oceanic waters on these shallow tropical shelves. River plumes, in turn, tend to be characterized by both a negative NEP and a preindustrial source of CO_2 to the atmosphere, as is simulated for the Amazon plume.

The extreme regional variability of the preindustrial shelf FCO_2 is best illustrated in the Arctic, where the contrasting Barents and Laptev Seas underline the individual and combined impacts of biogeochemical and physical processes on the FCO_2. In the Laptev Sea, substantial organic carbon inputs (Lacroix et al., 2020) are likely mineralized extensively on the shelf due to long water RTs (Table 1), causing a negative NEP over the region (Figures 6a and 6c), an occurrence also suggested in the study of Anderson et al. (2009). In addition, the extensive sea-ice cover (91%–92% yearly mean of sea-ice coverage), the low temperature and light limitation inhibit the biological productivity and the heat exchange in this regional sea. Thus, the Laptev Sea temperature decrease is buffered substantially in the wintertime (Pipko et al., 2017), a season which would otherwise favor CO_2 solubilization. The ice barrier in the Laptev Sea also implies that during the months of coldest temperatures, and therefore of largest potential CO_2 uptake, the CO_2 exchange with the atmosphere does not take place. These combined physical and biogeochemical effects result in a preindustrial CO_2 source of 1.7 $TgCyr^{-1}$ over the entire sea. At the opposite end of the pCO_2 spectrum (Figure 4), the Barents Sea is, to a large degree, ice-free during winter, causing a cooling of the oceanic inflows from the North Atlantic (Pipko et al., 2017), which strongly favors CO_2 uptake. The CO_2 exchange is furthermore not inhibited during the season, leading to markedly low pCO_2 levels both in the model, as well as in observations (Lauvset et al., 2013), and a stark preindustrial CO_2 uptake of 17 $TgCyr^{-1}$ in the region.

The model simulates a clear difference in the behavior of shallow and near-shore, and deeper outer shelf regions with respect to their FCO_2 (Figures 6d and 6e). For instance, continental shelves characterized by depths of 0–50 m act as a source of CO_2 to the atmosphere (0.02 $PgCyr^{-1}$), whereas deeper shelf regions with depths of between 50–150 and 150–250 m act as sinks of CO_2 in the model (−0.05 and −0.02 $PgCyr^{-1}$, respectively). The sinks found over the deeper shelves support the theory of Chen and Borges (2009), which suggest that most outer shelves with a large connection to the open ocean act as efficient CO_2 sinks since their water properties are majorly dictated by large nutrient inflows from the open ocean, thus the resulting

net autotrophy. In stark contrast, the atmospheric CO_2 sources found over nearshore, shallow shelves corroborate the traditional view of carbon cycling in the coastal ocean, in which terrigenous and in situ produced organic matter are thought to be efficiently resuspended and mineralized, leading to a CO_2 source for the atmosphere (e.g., Bauer et al., 2013; Mackenzie et al., 2004).

3.5. Implications for the Anthropogenic FCO_2

While the global continental shelf FCO_2 has been increasingly constrained on an observational basis, the baseline preindustrial air-sea CO_2 exchange is essentially unknown, hindering a robust quantitative assessment of the anthropogenic perturbation on the global shelf FCO_2. Studies using conceptual box models have suggested that the shelf FCO_2 switched from a source of up to 0.3 $PgCyr^{-1}$ (Andersson et al., 2005; Mackenzie et al., 2004, 2002, 2000; S. V. Smith & Hollibaugh, 1993; Ver et al., 1999), largely driven by the negative NEPs in the coastal ocean, to a contemporary sink of up to 0.4 $PgCyr^{-1}$, thus implying an anthropogenic perturbation of the continental shelf FCO_2 of as large as 0.7 $PgCyr^{-1}$. This anthropogenic uptake would contribute to 30% of the global ocean's anthropogenic CO_2 uptake. Derived from the difference between modeled present day (1998–2015 mean) and preindustrial states, our results suggest that the global continental shelf accounts for an anthropogenic CO_2 sink of 0.11 $PgCyr^{-1}$ only, which is consistent with the anthropogenic sink of 0.1 $PgCyr^{-1}$ estimated in the modeling study by Bourgeois et al. (2016). Our modeled anthropogenic CO_2 uptake, therefore, consists of only 5% of the global oceanic anthropogenic carbon uptake (2.1 $PgCyr^{-1}$), thus supporting the hypothesis that continental shelves, covering 7% of the total area in our model, are a slightly less efficient sink of CO_2 per unit area than the open ocean.

By computing long-term trends over 1800–2015, which was done to remove the impacts of decadal variability on the FCO_2, we find that areas exhibiting strong anthropogenic changes in FCO_2 per area were often already preindustrial CO_2 sinks per area (Figures 7a and 7b) in the model. In Bourgeois et al. (2016) and Liu et al. (2019), it is suggested that short water RTs are likely the main driver for the anthropogenic sink of CO_2. In our analysis, we show the simpler metric of the continental shelf sea floor depth might be a more important control factor for the anthropogenic CO_2 uptake (Figures 6d, 6e, and 7c), since our simulations show that areas without significant trends exhibit a mean depth of only 36 m, much shallower than the average depth of the global continental shelf (92 m). The relatively small volume of the continental shelves might therefore strongly limit the storage of anthropogenic carbon on the shelves, in contrast to in the deep ocean. In the open ocean, in contrast, the strongest carbon sinks are located in regions of convergence and formation of deep water, such as in the North Atlantic (Gruber et al., 2002).

While the observational study of Laruelle et al. (2018) recently suggested that the global continental shelf is more efficient at taking up anthropogenic CO_2 than the open ocean, it was also acknowledged in the study that Arctic shelves (25% of total shelf area in our model) and tropical shelves are currently severely undersampled. In our simulations, large areas of the Arctic shelf do not exhibit a significant historical trend in anthropogenic CO_2 uptake (Figure 7b), while sparsely sampled tropical regions, such as the Sunda Shelf, also tend to be inefficient areal sinks of anthropogenic CO_2. Thus, an analysis mostly based on midlatitude shelf regions, due to available current coverage from long time-series of pCO_2 observations, might overall be biased by overestimating the global shelf anthropogenic CO_2 uptake.

4. Model Limitations

The extent of continental shelves and the coastal ocean have been inconsistently defined in published literature (Borges et al., 2005; Laruelle et al., 2013, 2010, 2017; Walsh, 1991), which likely has an impact on their estimated contributions to the global NPP and FCO_2. For instance, Muller-Karger et al. (2005) use a coastal ocean definition including depths down to 2,000 m to derive a coastal contribution to the global NPP of around 30%, whereas less inclusive definitions lead to values closer to 10% (e.g., Gattuso et al., 1998). The global shelf used in our study accounts solely for the shallowest part of the ocean, where efficient pelagic-benthic coupling takes place and which is closer to the definition of Laruelle et al. (2013) based on a detailed analysis of the shelf break depth. Our definition partly affects the continental shelf FCO_2 estimated in this study, since we observe a stronger CO_2 sink at increasing depth threshold ranges (Figure 6d).

An adequate representation of oceanic currents and mixing is an important prerequisite to capture the biogeochemical dynamics on continental shelves. The spatial resolution of our simulation thus represents a significant improvement compared to many previous GOBM studies relying on grid-cell areas up to eight times larger in magnitude than used here (e.g., Giraud et al., 2008). The model configuration used here also provides a much more realistic representation of continental shelves than box models, which do not represent spatial gradients in physical and biogeochemical variables. By representing continental shelves in a global ocean model setup, as is done here, we avoid classical shortcomings of regional models due to imposing boundary conditions close to the shelf break, which may lead to drifts and inconsistencies stemming from applying boundary conditions to the model (Mathis et al., 2018). The model simulations shown here, nevertheless, have their own limitations, as they do not resolve spatial features on shelves to the same degree as regional models (e.g., Fennel & Wilkin, 2009; Frischknecht et al., 2018), and ignore fine-scale coastal dynamics induced by, for instance, tidal currents and eddies (e.g., Mathis et al., 2019). Eddies, for one, have been shown to play a nonnegligible role for carbon fluxes in eastern boundary upwelling systems (Gruber et al., 2011; Turi et al., 2016), but their contributions to the hydrodynamics on wide passive margins remain unclear. Furthermore, tidal waves and particulate resuspension, as described in the North Sea by Thomas et al. (2004) and Mathis et al. (2019), might favor CO_2 outgassing due to increased vertical mixing. The preindustrial sink simulated in our study is driven by the horizontal export of both organic and inorganic carbon, which could potentially be overestimated by not accounting for these processes that promote larger vertical mixing fluxes. The magnitude of this effect, however, has yet to be assessed in a global study. More broadly, significant uncertainties are introduced by the capacity of our model in representing the cross-shelf exchange. A regional study by Rutherford and Fennel (2018) suggests that the offshore export of shelf waters is generally inhibited by fine-scale circulation at the shelf break. While such an effect would directly have an impact on the NEP and FCO_2 estimates reported here, we do not find a systematic bias in our comparisons of modeled RTs with regional estimates, although the comparison is also somewhat blurred by the large uncertainties associated with these observations. Reduced inflows from the open ocean and reduced offshore export of material would be conducive to a weaker present-day shelf CO_2 sink. However, the 1998–2015 CO_2 sink in our simulations is lower than the most recent observation-based estimate of 0.2 ± 0.02 by Roobaert et al. (2019), and our simulated pCO_2 values are also generally higher than those of Laruelle et al. (2017), both suggesting that our model might actually have an outgassing bias over the global continental shelf.

Shallow coastal waters are important contributors to the global $CaCO_3$ production, due to particularly productive organisms such as corals, molluscs, foraminifera and red algae (Milliman & Droxler, 1996; Woodroffe et al., 2017). In our simulations, the benthic $CaCO_3$ production is, however, not explicitly represented, and, therefore, we likely underestimate the continental shelf $CaCO_3$ production, especially in areas such as the Sunda Shelf. Carbonate production impacts the FCO_2 through its impacts on alkalinity and DIC that lead to CO_2 production. We are, however, unable to assess the quantitative consequences of omitting shallow water benthic $CaCO_3$ production on the FCO_2 within the current state of our model and would recommend further model implementations in this direction, such as the representation of coral reef ecosystems.

The anthropogenic perturbation of the FCO_2 over the 20th century is also likely affected by the enhanced riverine supplies of DIP and DIN over the time period (Beusen et al., 2016; Seitzinger et al., 2010). This enhancement of nutrient inputs stimulates the coastal biological pump and was advocated to be a major control factor for the simulated source-sink switch in the FCO_2 by box model studies. Since we show here, however, that shelf water RTs are likely overestimated in these box-model studies, which would also apply to the shelf's exposure time to the nutrients, the impacts of increased nutrient inputs to the coastal ocean C cycle might, be smaller than is suggested in these studies.

5. Conclusions

To date, almost all aspects of the continental shelf carbon cycle remain poorly understood and quantified, with a possible exception of the present-day FCO_2. In this study, we present a comprehensive analysis of carbon fluxes on continental shelves for the preindustrial time period, and their evolutions as a response of contemporary changes to atmospheric CO_2 levels. To do this, we enhanced a GOBM, which accounts for 3D ocean circulation features, for land-to-ocean inputs, and for dynamic exchanges at the sediment, air-sea

and shelf-open ocean interfaces. Our results suggest that the preindustrial global continental shelf was both net autotrophic and a weak atmospheric CO_2 sink, in stark contrast to previous assessments based on box models, which have implied net heterotrophy and a CO_2 source to the atmosphere over the global shelf at preindustrial conditions. The disagreement regarding the sign of the trophic state and FCO_2 between these assessments and our study likely stems from the assumptions underlying the representation of oceanic inflows, which our analysis shows to be the main control of continental shelf water RTs. Indeed, the open ocean inflows appear to be responsible for extensive regions of both positive NEP and CO_2 uptake during the preindustrial time period by firstly providing the shelves with nutrients from open ocean subsurface waters, thus enhancing the NPP/NEP, and, second, reducing the RTs of waters, and thus of the newly produced organic matter, on the shelf. Our model shows that many large riverine freshwater plumes may also export terrigenous organic matter off the shelf rapidly due to their very short stratification-induced RTs on the shelf.

The features arising from our model's representation of spatial features on continental shelves could explain why the global continental shelf, as a whole, might actually be both net autotrophic and a sink of atmospheric CO_2 for the preindustrial time period, despite the global ocean being net heterotroph and a source of CO_2 to the atmosphere due to riverine inputs of terrestrial organic carbon and DIC to the ocean (Aumont et al., 2001; Friedlingstein et al., 2020; Lacroix et al., 2020; Resplandy et al., 2018). The shallow continental shelf of less than 50 m depth, while being subject to a stronger influence of riverine carbon inputs, is a source of carbon to the atmosphere in our simulations, but this source is completely offset by simulated net autotrophy on deeper outer shelves with depths of 50–250 m. The model, however, shows great spatial variability in sign and magnitude, and the regional fluxes are, at times, simulated to be as large as the global preindustrial FCO_2 (e.g., in the Barents Sea), emphasizing the importance of reducing uncertainties in the FCO_2 of individual regions, for which regional-scale studies are of central importance.

In previous GOBM studies, in which riverine loads are considered (e.g., Bernard et al., 2011; Bourgeois et al., 2016), terrestrial organic matter is assumed to be instantaneously degraded in the coastal ocean, leading to an instantaneous release of DIC. The present study is an improvement on this, for instance, through our explicit representation of the fate of tDOM in the ocean. Although our simulations show agreement with recent observational studies suggesting a relatively efficient transport of tDOM off the shelf, we still strongly simplify the chemical characterization and fate of terrestrial organic matter in the ocean due to the limited observational constraints and computing resources. Further improvements in the representation of the composition and dynamics of both terrestrial and marine organic matter in global ocean models is needed to reduce uncertainties for improving quantifications of the cycling of carbon on the global shelf.

In contrast to conceptual box model studies, our simulations explicitly account for the spatial variability in ocean circulation and biogeochemical dynamics on the shelves, albeit at a relatively coarse scale in comparison to regional models. This coarse model configuration might lead to considerable sources of uncertainties regarding the carbon dynamics in the near-shore coastal ocean, in river plumes or in regions strongly impacted by eddies. In the future, advances in computing power and further model developments may permit an evaluation of the global shelf carbon cycle in a fully eddy-resolving model, for which the results of our study can serve as a benchmark. As of now, our model results emphasize the importance of open ocean inflows for carbon fluxes on the global continental shelf. This is why we stress the importance of evaluating the continental shelf as a nonenclosed system with 3D dynamical boundaries to assess changes in the cycling of carbon associated with this shallow segment of the ocean.

Data Availability Statement

Raw data of the continental shelves results from the simulations are available under https://doi.org/10.17882/72614.

References

Aarnos, H., Gélinas, Y., Kasurinen, V., Gu, Y., Puupponen, V.-M., & Vähätalo, A. V. (2018). Photochemical mineralization of terrigenous DOC to dissolved inorganic carbon in ocean. *Global Biogeochemical Cycles*, *32*, 250–266. https://doi.org/10.1002/2017GB005698

Anderson, L. G., Jutterström, S., Hjalmarsson, S., Wåhlström, I., & Semiletov, I. (2009). Out-gassing of CO_2 from Siberian Shelf seas by terrestrial organic matter decomposition. *Geophysical Research Letters*, *36*, L20601. https://doi.org/10.1029/2009GL040046

Acknowledgments
All simulations were performed at the German Climate Computing Center (DKRZ). F. Lacroix received funding from the European Union's Horizon 2020 research and innovation program under the Marie Skłodowska-Curie Grant agreement no. 643052 (C-CASCADES project). F. Lacroix and T. Ilyina received were supported by the European Union's Horizon 2020 research and innovation program under Grant agreement no. 641816 (CRESCENDO) and under Grant agreement no. 821003 (4C), as well as by the German paleo-climate modeling initiative PalMod (FKZ: 01LP1505A, 01LP1515C). PalMod is part of the Research for Sustainable Development initiative (FONA) funded by the German Federal Ministry of Education and Research (BMBF). T. Ilyina was supported by the Deutsche Forschungsgemeinschaft (DFG, German Research Foundation) under Germany's Excellence Strategy—EXC 2037 "Climate, Climatic Change, and Society"—Project Number: 390683824. P. Regnier received financial support from BELSPO through the project ReCAP, which is part of the Belgian research program FedTwin. G. G. Laruelle received funding under European Union's Horizon 2020 research and innovation program grant agreement no. 776810 (VERIFY project). The authors thank the manuscript's editor K. Matsumoto, and reviewers T. Bourgeois, J. Lauderdale, along with two further anonymous reviewers for their constructive and helpful contributions to our study.

Andersson, A. J., Mackenzie, F., & Lerman, A. (2005). Coastal ocean and carbonate systems in the high CO_2 world of the Anthropocene. *American Journal of Science*, *305*, 875–918. https://doi.org/10.2475/ajs.305.9.875

Arndt, S., Jørgensen, B. B., LaRowe, D. E., Middelburg, J. J., Pancost, R. D., & Regnier, P. (2013). Quantifying the degradation of organic matter in marine sediments: A review and synthesis. *Earth-Science Reviews*, *123*, 53–86. https://doi.org/10.1016/j.earscirev.2013.02.008

Aumont, O., Orr, J. C., Monfray, P., Ludwig, W., Amiotte-Suchet, P., & Probst, J.-L. (2001). Riverine-driven interhemispheric transport of carbon. *Global Biogeochemical Cycles*, *15*(2), 393–405. https://doi.org/10.1029/1999GB001238

Bakker, D. C. E., Pfeil, B., Landa, C. S., Metzl, N., O'Brien, K. M., Olsen, A., et al. (2016). A multi-decade record of high-quality fCO_2 data in version 3 of the Surface Ocean CO_2 Atlas (SOCAT). *Earth System Science Data*, *8*, 383–413. https://doi.org/10.5194/essd-8-383-2016

Bauer, J. E., Cai, W.-J., Raymond, P. A., Bianchi, T. S., Hopkinson, C. S., & Regnier, P. A. G. (2013). The changing carbon cycle of the coastal ocean. *Nature*, *504*, 61.

Behrenfeld, M. J., Randerson, J. T., McClain, C. R., Feldman, G. C., Los, S. O., Tucker, C. J., et al. (2001). Biospheric primary production during an ENSO transition. *Science*, *291*(5513), 2594–2597. https://doi.org/10.1126/science.1055071

Benner, R., Louchouarn, P., & Amon, R. M. W. (2005). Terrigenous dissolved organic matter in the Arctic Ocean and its transport to surface and deep waters of the North Atlantic. *Global Biogeochemical Cycles*, *19*, GB2025. https://doi.org/10.1029/2004GB002398

Bernard, C. Y., Dürr, H. H., Heinze, C., Segschneider, J., & Maier-Reimer, E. (2011). Contribution of riverine nutrients to the silicon biogeochemistry of the global ocean—A model study. *Biogeosciences*, *8*, 551–564. https://doi.org/10.5194/bg-8-551-2011

Beusen, A. H. W., Bouwman, A. F., Van Beek, L. P. H., Mogollón, J. M., & Middelburg, J. J. (2016). Global riverine N and P transport to ocean increased during the 20th century despite increased retention along the aquatic continuum. *Biogeosciences*, *13*, 2441–2451. https://doi.org/10.5194/bg-13-2441-2016

Blaas, M., Kerkhoven, D., & de Swart, H. (2001). Large-scale circulation and flushing characteristics of the North Sea under various climate forcings. *Climate Research*, *18*, 47–54. https://doi.org/10.3354/cr018047

Borges, A. V., Delille, B., & Frankignoulle, M. (2005). Budgeting sinks and sources of CO_2 in the coastal ocean: Diversity of ecosystems counts. *Geophysical Research Letters*, *32*, L14601. https://doi.org/10.1029/2005GL023053

Bourgeois, T., Orr, J. C., Resplandy, L., Terhaar, J., Ethé, C., Gehlen, M., & Bopp, L. (2016). Coastal-ocean uptake of anthropogenic carbon. *Biogeosciences*, *13*, 4167–4185. https://doi.org/10.5194/bg-13-4167-2016

Cai, W.-J. (2011). Estuarine and coastal ocean carbon paradox: CO_2 sinks or sites of terrestrial carbon incineration?. *Annual Review of Marine Science*, *3*, 123–145. https://doi.org/10.1146/annurev-marine-120709-142723

Cai, W.-J., Pomeroy, L. R., Moran, M. A., & Wang, Y. (1999). Oxygen and carbon dioxide mass balance for the estuarine-intertidal marsh complex of five rivers in the southeastern U.S. *Limnology & Oceanography*, *44*, 639–649. https://doi.org/10.4319/lo.1999.44.3.0639

Carr, M.-E., Friedrichs, M. A. M., Schmeltz, M., Aita, M. N., Antoine, D., Arrigo, K. R., & Asanuma, I. (2006). A comparison of global estimates of marine primary production from ocean color. *Deep Sea Research Part II: Topical Studies in Oceanography*, *53*, 741–770. https://doi.org/10.1016/j.dsr2.2006.01.028

Chen, C.-T. A., & Borges, A. (2009). Reconciling opposing views on carbon cycling in the coastal ocean: Continental shelves as sinks and nearshore ecosystems as sources of atmospheric CO_2. *Deep Sea Research Part II: Topical Studies in Oceanography*, *56*, 578–590. https://doi.org/10.1016/j.dsr2.2009.01.001

Combes, V., & Matano, R. (2018). The Patagonian shelf circulation: Drivers and variability. *Progress in Oceanography*, *167*, 24–43. https://doi.org/10.1016/j.pocean.2018.07.003

Crossland, C., Baird, D., Ducrotoy, J.-P., Lindeboom, H., Buddemeier, W. R., Dennison, W., et al. (2006). The coastal zone—A domain of global interactions. In C. J. Crossland, H. H. Kremer, H. J. Lindeboom, J. I. Marshall Crossland, & M. D. A. Le Tissier (Eds), *Coastal fluxes in the anthropocene* (pp. 1–37). Springer. https://doi.org/10.1007/3-540-27851-6_1

DeVries, T., & Weber, T. (2017). The export and fate of organic matter in the ocean: New constraints from combining satellite and oceanographic tracer observations. *Global Biogeochemical Cycles*, *31*, 535–555. https://doi.org/10.1002/2016GB005551

Eicken, H., Dmitrenko, I., Tyshko, K., Darovskikh, A., Dierking, W., Blahak, U., et al. (2005). Zonation of the Laptev Sea landfast ice cover and its importance in a frozen estuary. *Global and Planetary Change*, *48*, 55–83. https://doi.org/10.1016/j.gloplacha.2004.12.005

Etheridge, D. M., Steele, L. P., Langenfelds, R. L., Francey, R. J., Barnola, J.-M., & Morgan, V. I. (1996). Natural and anthropogenic changes in atmospheric CO_2 over the last 1000 years from air in Antarctic ice and firn. *Journal of Geophysical Research*, *101*, 4115–4128. https://doi.org/10.1029/95JD03410

Fekete, B. M., Vörösmarty, C. J., & Grabs, W. (2002). High-resolution fields of global runoff combining observed river discharge and simulated water balances. *Global Biogeochemical Cycles*, *16*, 10–15. https://doi.org/10.1029/1999GB001254

Fennel, K., Alin, S., Barbero, L., Evans, W., Bourgeois, T., Cooley, et al. (2019). Carbon cycling in the North American coastal ocean: A synthesis. *Biogeosciences*, *16*, 1281–1304. https://doi.org/10.5194/bg-16-1281-2019

Fennel, K., & Testa, J. M. (2019) Biogeochemical controls on coastal hypoxia. *Annual Review of Marine Science*, *11*, 105–130. https://doi.org/10.1146/annurev-marine-010318-095138

Fennel, K., & Wilkin, J. (2009). Quantifying biological carbon export for the northwest North Atlantic continental shelves. *Geophysical Research Letters*, *36*, L18605. https://doi.org/10.1029/2009GL039818

Fichot, C. G., & Benner, R. (2014). The fate of terrigenous dissolved organic carbon in a river-influenced ocean margin. *Global Biogeochemical Cycles*, *28*, 300–318. https://doi.org/10.1002/2013GB004670

Friedlingstein, P., O'Sullivan, M., Jones, M. W., Andrew, R. M., Hauck, J., Olsen, J., et al. (2020). Global carbon budget 2020. *Earth System Data*, *12*, 3269–3240. https://doi.org/10.5194/essd-12-3269-2020

Frischknecht, M., Münnich, M., & Gruber, N. (2018). Origin, transformation, and fate: The three-dimensional biological pump in the California Current System. *Journal of Geophysical Research: Oceans*, *123*, 7939–7962. https://doi.org/10.1029/2018JC013934

Gattuso, J.-P., Frankignoulle, M., & Wollast, R. (1998). Carbon and carbonate metabolism in coastal aquatic ecosystems. *Annual Review of Ecology and Systematics*, *29*, 405–434. https://doi.org/10.1146/annurev.ecolsys.29.1.405

Giraud, X., Le Quéré, C., & da Cunha, L. C. (2008). Importance of coastal nutrient supply for global ocean biogeochemistry. *Global Biogeochemical Cycles*, *22*, GB2025. https://doi.org/10.1029/2006GB002717

Gong, D., Kohut, J. T., & Glenn, S. M. (2010). Seasonal climatology of wind-driven circulation on the New Jersey Shelf. *Journal of Geophysical Research*, *115*, C04006. https://doi.org/10.1029/2009JC005520

Griffies, S. M., Danabasoglu, G., Durack, P. J., Adcroft, A. J., Balaji, V., Böning, C. W., et al. (2016). OMIP contribution to CMIP6: Experimental and diagnostic protocol for the physical component of the Ocean Model Intercomparison Project. *Geoscientific Model Development*, *9*, 3231–3296. https://doi.org/10.5194/gmd-9-3231-2016

Gruber, N., Keeling, C. D., & Bates, N. R. (2002). Interannual variability in the North Atlantic Ocean Carbon sink. *Science*, *298*, 2374–2378. https://doi.org/10.1126/science.1077077

Gruber, N., Lachkar, Z., Frenzel, H., Marchesiello, P., Münnich, M., McWilliams, J. C., et al. (2011). Eddy-induced reduction of biological production in eastern boundary upwelling systems. *Nature Geoscience*, *4*, 787.

Hancock, G., Webster, I., & Stieglitz, T. (2006). Horizontal mixing of Great Barrier Reef waters: Offshore diffusivity determined from radium isotope distribution. *Journal of Geophysical Research*, *111*, C12019. https://doi.org/10.1029/2006JC003608

Heinze, C., & Maier-Reimer, E. (1999). *The Hamburg oceanic carbony cycle circulation model version "HAMOCC2s" for long time integrations* (Technical Report 20). Deutsches Klimarechenzentrum, Hamburg: Modellberatungsgruppe.

Henson, S. A., Sanders, R., Madsen, E., Morris, P. J., Le Moigne, F., & Quartly, G. D. (2011). A reduced estimate of the strength of the ocean's biological carbon pump. *Geophysical Research Letters*, *38*, L04606. https://doi.org/10.1029/2011GL046735

Hernes, P. J., & Benner, R. (2002). Transport and diagenesis of dissolved and particulate terrigenous organic matter in the North Pacific Ocean. *Deep Sea Research Part I: Oceanographic Research Papers*, *49*, 2119–2132. https://doi.org/10.1016/S0967-0637(02)001280

Huthnance, J. M. (1997). North sea interaction with the North Atlantic Ocean. *Deutsche Hydrografische Zeitschrift*, *49*, 153–162. https://doi.org/10.1007/BF02764030

Ilyina, T., Six, K. D., Segschneider, J., Maier-Reimer, E., Li, H., & Núñez-Riboni, I. (2013). Global ocean biogeochemistry model HAMOCC: Model architecture and performance as component of the MPI-Earth system model in different CMIP5 experimental realizations. *Journal of Advances in Modeling Earth Systems*, *5*, 287–315. https://doi.org/10.1029/2012MS000178

Ittekkot, V. (1988). Global trends in the nature of organic matter in river suspensions. *Nature*, *332*, 436.

Izett, J. G., & Fennel, K. (2018). Estimating the cross-shelf export of riverine materials: Part 1. General relationships from an idealized numerical model. *Global Biogeochemical Cycles*, *32*, 160–175. https://doi.org/10.1002/2017GB005667

Jacobson, A. R., Mikaloff Fletcher, S. E., Gruber, N., Sarmiento, J. L., & Gloor, M. (2007). A joint atmosphere-ocean inversion for surface fluxes of carbon dioxide: 1. Methods and global-scale fluxes. *Global Biogeochemical Cycles*, *21*, GB1019. https://doi.org/10.1029/2005GB002556

Johnson, K. S., Chavez, F. P., & Friederich, G. E. (1999). Continental-shelf sediment as a primary source of iron for coastal phytoplankton. *Nature*, *398*, 697. https://doi.org/10.1038/19511http://10.0.4.14/19511

Jungclaus, J. H., Fischer, N., Haak, H., Lohmann, K., Marotzke, J., Matei, D., et al. (2013). Characteristics of the ocean simulations in the Max Planck Institute Ocean Model (MPI-OM) the ocean component of the MPI-Earth system model. *Journal of Advances in Modeling Earth Systems*, *5*, 422–446. https://doi.org/10.1002/jame.20023

Kaiser, K., Benner, R., & Amon, R. M. W. (2017). The fate of terrigenous dissolved organic carbon on the Eurasian shelves and export to the North Atlantic. *Scientific Reports*, *7*, 13064. https://doi.org/10.1038/s41598-017-12729-1

Krumins, V., Gehlen, M., Arndt, S., Van Cappellen, P., & Regnier, P. (2013). Dissolved inorganic carbon and alkalinity fluxes from coastal marine sediments: Model estimates for different shelf environments and sensitivity to global change. *Biogeosciences*, *10*, 371–398. https://doi.org/10.5194/bg-10-371-2013

Lacroix, F., Ilyina, T., & Hartmann, J. (2020). Oceanic CO_2 outgassing and biological production hotspots induced by pre-industrial river loads of nutrients and carbon in a global modeling approach. *Biogeosciences*, *17*, 55–88. https://doi.org/10.5194/bg-17-55-2020

Laruelle, G. G., Cai, W.-J., Hu, X., Gruber, N., Mackenzie, F. T., & Regnier, P. (2018). Continental shelves as a variable but increasing global sink for atmospheric carbon dioxide. *Nature Communications*, *9*, 454. https://doi.org/10.1038/s41467-017-02738-z

Laruelle, G. G., Dürr, H. H., Lauerwald, R., Hartmann, J., Slomp, C. P., Goossens, N., & Regnier, P. A. G. (2013). Global multi-scale segmentation of continental and coastal waters from the watersheds to the continental margins. *Hydrology and Earth System Sciences*, *17*, 2029–2051. https://doi.org/10.5194/hess-17-2029-2013

Laruelle, G. G., Dürr, H. H., Slomp, C. P., & Borges, A. V. (2010). Evaluation of sinks and sources of CO_2 in the global coastal ocean using a spatially-explicit typology of estuaries and continental shelves. *Geophysical Research Letters*, *37*, L15607. https://doi.org/10.1029/2010GL043691

Laruelle, G. G., Landschützer, P., Gruber, N., Tison, J.-L., Delille, B., & Regnier, P. (2017). Global high-resolution monthly pCO_2 climatology for the coastal ocean derived from neural network interpolation. *Biogeosciences*, *14*, 4545–4561. https://doi.org/10.5194/bg-14-4545-2017

Laruelle, G. G., Lauerwald, R., Pfeil, B., & Regnier, P. (2014). Regionalized global budget of the CO_2 exchange at the air-water interface in continental shelf seas. *Global Biogeochemical Cycles*, 1199–1214. https://doi.org/10.1002/2014GB004832

Lauvset, S. K., Chierici, M., Counillon, F., Omar, A., Nondal, G., Johannessen, T., & Olsen, A. (2013). Annual and seasonal fCO_2 and air–sea CO_2 fluxes in the Barents Sea. *Journal of Marine Systems*, *113–114*, 62–74. https://doi.org/10.1016/j.jmarsys.2012.12.011

Liu, X., Dunne, J. P., Stock, C. A., Harrison, M. J., Adcroft, A., & Resplandy, L. (2019). Simulating water residence time in the coastal ocean: A global perspective. *Geophysical Research Letters*, *46*, 13910–13919. https://doi.org/10.1029/2019GL085097

Loder, J. W. (1993). *The coastal ocean off northeastern North America: A large-scale view*. In A. R. Robinson, & K. H. Brink (Eds.), The Sea. 11 (pp. 105–138). Wiley.

Mackenzie, F. T., Lerman, A., & Andersson, A. J. (2004). Past and present of sediment and carbon biogeochemical cycling models. *Biogeosciences*, *1*, 11–32. https://doi.org/10.5194/bg-1-11-2004

Mackenzie, F. T., Lerman, A., & Ver, L. M. B. (1998). Role of the continental margin in the global carbon balance during the past three centuries. *Geology*, *26*, 423–426.

Mackenzie, F. T., Ver, L. M., & Lerman, A. (2000). Coastal-zone biogeochemical dynamics under global warming. *International Geology Review*, *42*, 193–206. https://doi.org/10.1080/00206810009465077

Mackenzie, F. T., Ver, L. M., & Lerman, A. (2002). Century-scale nitrogen and phosphorus controls of the carbon cycle. *Chemical Geology*, *190*, 13–32. https://doi.org/10.1016/S0009-2541(02)00108-0

Maier-Reimer, E., & Hasselmann, K. (1987). Transport and storage of CO_2 in the ocean—An inorganic ocean-circulation carbon cycle model. *Climate Dynamics*, *2*, 63–90. https://doi.org/10.1007/BF01054491

Mathis, M., Elizalde, A., & Mikolajewicz, U. (2018). Which complexity of regional climate system models is essential for downscaling anthropogenic climate change in the Northwest European Shelf? *Climate Dynamics*, *50*, 2637–2659. https://doi.org/10.1007/s00382-017-3761-3

Mathis, M., Elizalde, A., & Mikolajewicz, U. (2019). The future regime of Atlantic nutrient supply to the Northwest European Shelf. *Journal of Marine Systems*, *189*, 98–115. https://doi.org/10.1016/j.marsys.2018.10.002

Mathis, M., Mayer, B., & Pohlmann, T. (2013). An uncoupled dynamical downscaling for the North sea: Method and evaluation. *Ocean Modelling*, *72*, 153–166. https://doi.org/10.1016/j.ocemod.2013.09.004

Mauritsen, T., Bader, J., Becker, T., Behrens, J., Bittner, M., Brokopf, R., et al. (2019). Developments in the MPI-M Earth system model version 1.2 (MPI-ESM 1.2) and its response to increasing CO_2. *Journal of Advances in Modeling Earth Systems*, *11*, 998–1038. https://doi.org/10.1029/2018MS001400

Mayer, B., Stacke, T., Stottmeister, I., & Pohlmann, T. (2015). Sunda shelf seas: Flushing rates and residence times. *Ocean Science*, *12*, 863–895. https://doi.org/10.5194/osd-12-863-2015

Meijers, A. J. S. (2014). The Southern Ocean in the coupled model intercomparison project phase 5. *Philosophical Transactions of The Royal Society A: Mathematical Physical and Engineering Sciences*, *372*, 20130296.
Men, W., & Liu, G. (2015). Distribution of ^{226}Ra and the residence time of the shelf water in the Yellow Sea and the East China Sea. *Journal of Radioanalytical and Nuclear Chemistry*, *303*, 2333–2344. https://doi.org/10.1007/s10967-014-3749-y
Meybeck, M. (1982). Carbon, nitrogen, and phosphorus transport by world rivers. *American Journal of Science*, *282*, 401–450.
Meybeck, M., & Vörösmarty, C. (1999). Global transfer of carbon by rivers. *Global Change News Letter*, *26*, 18–19.
Milliman, J. D., & Droxler, A. W. (1996). Neritic and pelagic carbonate sedimentation in the marine environment: Ignorance is not bliss. *Geologische Rundschau*, *85*, 496–504. https://doi.org/10.1007/BF02369004
Monsen, N. E., Cloern, J. E., Lucas, L. V., & Monismith, S. G. (2002). A comment on the use of flushing time, residence time, and age as transport time scales. *Limnology & Oceanography*, *47*, 1545–1553. https://dx.doi.org/10.4319/lo.2002.47.5.1545
Moore, W. S., & de Oliveira, J. (2008). Determination of residence time and mixing processes of the Ubatuba, Brazil, inner shelf waters using natural Ra isotopes. *Estuarine. Coastal and Shelf Science*, *76*, 512–521. http://www.sciencedirect.com/science/article/pii/S0272771407003046
Muller-Karger, F. E., Varela, R., Thunell, R., Luerssen, R., Hu, C., & Walsh, J. J. (2005). The importance of continental margins in the global carbon cycle. *Geophysical Research Letters*, *32*. https://doi.org/10.1029/2004GL021346
Nozaki, Y., Kasemsupaya, V., & Tsubota, H. (1989). Mean residence time of the shelf water in the East China and the Yellow Seas determined by ^{228}Ra/^{226}Ra measurements. *Geophysical Research Letters*, *16*, 1297–1300. https://doi.org/10.1029/GL016i011p01297
Opsahl, S., & Benner, R. (1997). Distribution and cycling of terrigenous dissolved organic matter in the ocean. *Nature*, *386*, 480–482. https://doi.org/10.1038/386480a0
Orr, J. C., Najjar, R. G., Aumont, O., Bopp, L., Bullister, J. L., Danabasoglu, G., et al. (2017). Biogeochemical protocols and diagnostics for the CMIP6 Ocean Model Intercomparison Project (OMIP). *Geoscientific Model Development*, *10*(6), 2169–2199. http://dx.doi.org/10.5194/gmd-10-2169-2017
Painter, S. C., Lapworth, D. J., Woodward, E., Kroeger, S., Evans, C. D., Mayor, D., & Sanders, R. (2018). Terrestrial dissolved organic matter distribution in the North Sea. *Science of the Total Environment*, *630*, 630–647. https://doi.org/10.1016/j.scitotenv.2018.02.237
Pätsch, J., Kühn, W., & Six,K. D. (2018). Interannual sedimentary effluxes of alkalinity in the southern North Sea: Model results compared with summer observations, *Biogeosciences*, *15*, 3293–3309. https://doi.org/10.5194/bg-15-3293-2018
Paulsen, H., Ilyina, T., Six, K. D., & Stemmler, I. (2017). Incorporating a prognostic representation of marine nitrogen fixers into the Global Ocean Biogeochemical Model HAMOCC. *Journal of Advances in Modeling Earth Systems*, *9*, 438–464. https://doi.org/10.1002/2016MS000737
Pipko, I. I., Pugach, S. P., Semiletov, I. P., Anderson, L. G., Shakhova, N. E., Gustafsson, O., et al. (2017). The spatial and interannual dynamics of the surface water carbonate system and air–sea CO_2 fluxes in the outer shelf and slope of the Eurasian Arctic Ocean. *Ocean Science*, *13*, 997–1016. https://doi.org/10.5194/os-13-997-2017
Poli, P., Hersbach, H., & Dee, D. P. (2016). ERA-20C: An atmospheric reanalysis of the twentieth century. *Journal of Climate*, *29*, 4083–4097. https://doi.org/10.1175/JCLI-D-15-0556.1
Qiao, F., Yang, Y., Lü, X., Xia, C., Chen, X., Wang, B., & Yuan, Y. (2006). Coastal upwelling in the East China sea in winter. *Journal of Geophysical Research*, *111*, C11S06. https://doi.org/10.1029/2005JC003264
Rabalais, N. N., Turner, R. E., & Wiseman, W. J. (2002). Gulf of Mexico Hypoxia, A.K.A. "The dead zone". *Annual Review of Ecology and Systematics*, *33*, 235–263. https://doi.org/10.1146/annurev.ecolsys.33.010802.150513
Rabouille, C., Mackenzie, F. T., & Ver, L. M. (2001). Influence of the human perturbation on carbon, nitrogen, and oxygen biogeochemical cycles in the global coastal ocean. *Geochimica et Cosmochimica Acta*, *65*, 3615–3641. https://doi.org/10.1016/S00167037(01)00760-8
Radach, G., & Pätsch, J. (2007). Variability of continental riverine freshwater and nutrient inputs into the North Sea for the years 1977–2000 and its consequences for the assessment of eutrophication. *Estuaries and Coasts*, *30*, 66–81. https://doi.org/10.1007/BF02782968
Regnier, P., Friedlingstein, P., Ciais, P., Mackenzie, F., Gruber, N., Jansens, I., et al. (2013). Anthropogenic perturbation of the carbon fluxes from land to ocean. *Nature Geoscience*, *6*, 597–607.
Ren, J. L., Zhang, J., Li, J. B., Yu, X. Y., Liu, S. M., & Zhang, E. R. (2006). Dissolved aluminum in the Yellow sea and East China sea – Al as a tracer of Changjiang (Yangtze River) discharge and Kuroshio incursion. *Estuarine, Coastal and Shelf Science*, *68*, 165–174. https://doi.org/10.1016/j.ecss.2006.02.004
Resplandy, L., Keeling, R. F., Rödenbeck, C., Stephens, B. B., Khatiwala, S., Rodgers, K. B., et al. (2018). Revision of global carbon fluxes based on a reassessment of oceanic and riverine carbon transport. *Nature Geoscience*, *11*, 504–509. https://doi.org/10.1038/s41561-018-0151-3
Roobaert, A., Laruelle, G. G., Landschützer, P., Gruber, N., Chou, L., & Regnier, P. (2019). The spatiotemporal dynamics of the sources and sinks of CO_2 in the global coastal ocean. *Global Biogeochemical Cycles*, *33*, 1693–1714. https://doi.org/10.1029/2019GB006239
Rutherford, K., & Fennel, K. (2018). Diagnosing transit times on the northwestern North Atlantic continental shelf. *Ocean Science*, *14*, 1207–1221. https://doi.org/10.5194/os-14-1207-2018
Saba, V. S., Friedrichs, M. A. M., Antoine, D., Armstrong, R. A., Asanuma, I., Behrenfeld, M. J., et al. (2011). An evaluation of ocean color model estimates of marine primary productivity in coastal and pelagic regions across the globe. *Biogeosciences*, *8*, 489–503. https://doi.org/10.5194/bg-8-489-2011
Sarin, M. M., Rengarajan, R., & Somayajulu, B. L. K. (1994). Natural radionuclides in the Arabian Sea and Bay of Bengal: Distribution and evaluation of particle scavenging processes. *Earth and Planetary Sciences*, *103*, 211–235. https://doi.org/10.1007/BF02839537
Sarmiento, J., & Sundquist, E. (1992). Revised budget for the oceanic uptake of anthropogenic carbon dioxide. *Nature*, *356*, 589–593. https://doi.org/10.1038/356589a0
Schlosser, P., Bauch, D., Fairbanks, R., & Bönisch, G. (1994). Arctic river-runoff: Mean residence time on the shelves and in the halocline. *Deep Sea Research Part 1: Oceanographic Research Papers*, *41*, 1053–1068. https://doi.org/10.1016/0967-0637(94)90018-3
Seitzinger, S. P., Mayorga, E., Bouwman, A. F., Kroeze, C., Beusen, A. H. W., Billen, G., et al. (2010). Global river nutrient export: A scenario analysis of past and future trends. *Global Biogeochemical Cycles*, *24*, GB0A08. https://doi.org/10.1029/2009GB003587
Semiletov, I. P., Shakhova, N. E., Pipko, I. I., Pugach, S. P., Charkin, A. N., Dudarev, O. V., et al. (2013). Space-time dynamics of carbon and environmental parameters related to carbon dioxide emissions in the Buor-Khaya Bay and adjacent part of the Laptev Sea. *Biogeosciences*, *10*, 5977–5996. https://doi.org/10.5194/bg-10-5977-2013
Sharples, J., Middelburg, J. J., Fennel, K., & Jickells, T. D. (2017). What proportion of riverine nutrients reaches the open ocean?. *Global Biogeochemical Cycles*, *31*, 39–58. https://doi.org/10.1002/2016GB005483
Six, K. D., & Maier-Reimer, E. (1996). Effects of plankton dynamics on seasonal carbon fluxes in an ocean general circulation model. *Global Biogeochemical Cycles*, *10*, 559–583. https://doi.org/10.1029/96GB02561

Smith, R. C., Bidigare, R. R., Prézelin, B. B., Baker, K. S., & Brooks, J. M. (1987). Optical characterization of primary productivity across a coastal front. *Marine Biology*, *96*, 575–591. https://doi.org/10.1007/BF00397976

Smith, S. V., & Hollibaugh, J. T. (1993). Coastal metabolism and the oceanic organic carbon balance. *Reviews of Geophysics*, *31*, 75–89. https://doi.org/10.1029/92RG02584

Song, H., Marshall, J., Follows, M. J., Dutkiewicz, S., & Forget, G. (2016). Source waters for the highly productive Patagonian shelf in the southwestern Atlantic. *Journal of Marine Systems*, *158*, 120–128. https://doi.org/10.1016/j.jmarsys.2016.02.009

Takahashi, T., Wallace, S. B., & Langer, S. (1985). Redfield ratio based on chemical data from isopycnal surfaces. *Journal of Geophysical Research*, *90*, 6907–6924. https://doi.org/10.1029/JC090iC04p06907

Thomas, H., Bozec, Y., de Baar, H. J. W., Elkalay, K., Frankignoulle, M., Schiettecatte, L.-S., et al. (2005). The carbon budget of the North Sea. *Biogeosciences*, *2*, 87–96. https://doi.org/10.5194/bg-2-87-2005

Thomas, H., Bozec, Y., Elkalay, K., & De Baar, H. (2004). Enhanced open ocean storage of CO_2 from shelf sea pumping. *Science*, *304*, 1005–1008.

Turi, G., Lachkar, Z., Gruber, N., & Münnich, M. (2016). Climatic modulation of recent trends in ocean acidification in the California Current System. *Environmental Research Letters*, *11*, 14007. https://doi.org/10.1088/1748-9326/11/1/014007

Tyrrell, T. (1999). The relative influences of nitrogen and phosphorus on oceanic primary production. *Nature*, *400*, 525–531. https://doi.org/10.1038/22941

US Department of Commerce and Atmospheric Administration (2006). *N. G. D. C. ETOPO2*. http://www.ngdc.noaa.gov/mgg/fliers/06mgg01.html

Ver, L. M. B., Mackenzie, F. T., & Lerman, A. (1999). Carbon cycle in the coastal zone: Effects of global perturbations and change in the past three centuries. *Chemical Geology*, *159*, 283–304. https://doi.org/10.1016/S0009-2541(99)00042-X

Vodacek, A., Blough, N. V., DeGrandpre, M. D., DeGrandpre, M. D., & Nelson, R. K. (2003). Seasonal variation of CDOM and DOC in the Middle Atlantic Bight: Terrestrial inputs and photooxidation. *Limnology & Oceanography*, *42*, 674–686. https://doi.org/10.4319/lo.1997.42.4.0674

Walsh, J. J. (1988). *On the Nature of Continental Shelves* (1st ed., pp. 1–528). New York, NY: Elsevier. https://www.elsevier.com/books/on-the-nature-of-continental-shelves/walsh/978-0-12-733775-3

Walsh, J. J. (1991). Importance of continental margins in the marine biogeochemical cycling of carbon and nitrogen. *Nature*, *350*, 53–55. https://doi.org/10.1038/350053a0

Wang, J., Yan, W., Chen, N., Li, X., & Liu, L. (2015). Modeled long-term changes of DIN:DIP ratio in the Changjiang River in relation to Chl-α and DO concentrations in adjacent estuary. *Estuarine, Coastal and Shelf Science*, *166*, 153–160.

Wanninkhof, R., Park, G.-H., Takahashi, T., Sweeney, C., Feely, R., Nojiri, Y., et al. (2013). Global ocean carbon uptake: Magnitude, variability and trends. *Biogeosciences*, *10*, 1983–2000. https://doi.org/10.5194/bg-10-1983-2013

Wollast, R., & Chou, L. (1998). Distribution and fluxes of calcium carbonate along the continental margin in the Gulf of Biscay. *Aquatic Geochemistry*, *4*, 369–393. https://doi.org/10.1023/A:1009640432692

Woodroffe, C. D., Farell, J. W., Hall, F. R., & Harris, P. T. (2017). Calcium carbonate production and contribution to coastal sediments. *The First Global Integrated Marine Assessment: World Ocean Assessment I*, 149–158. 10.1017/9781108186148.010

Yamamoto, M., Tanaka, N., & Tsunogai, S. (2001). Okhotsk Sea intermediate water formation deduced from oxygen isotope systematics. *Journal of Geophysical Research*, *106*, 31075–31084.

Yasuda, I., Kouketsu, S., Katsumata, K., Ohiwa, M., Kawasaki, Y., & Kusaka, A. (2002). Influence of Okhotsk sea intermediate water on the Oyashio and North Pacific intermediate water. *Journal of Geophysical Research*, *107*, 11–30. https://doi.org/10.1029/2001JC001037

Zhou, F., Xue, H., Huang, D., Xuan, J., Ni, X., Xiu, P., & Hao, Q. (2015). Cross-shelf exchange in the shelf of the East China Sea. *Journal of Geophysical Research: Oceans*, *120*, 1545–1572. https://doi.org/10.1002/2014JC010567